UNIVERSIDADE ESTADUAL DE CAMPINAS

FACULDADE DE ENGENHARIA MECÂNICA

E INSTITUTO DE GEOCIÊNCIAS

GEORGE HANS STERLING MORA

RHEOLOGICAL AND STATISTICAL STUDIES OF A SHEAR-SENSITIVE FLUID TO CONTROL CIRCULATION LOSS

ESTUDOS REOLÓGICO E ESTATÍSTICO DE UM FLUIDO SENSÍVEL AO CISALHAMENTO PARA CONTROLAR PERDAS DE CIRCULAÇÃO

CAMPINAS

2020

GEORGE HANS STERLING MORA

RHEOLOGICAL AND STATISTICAL STUDIES OF A SHEAR-SENSITIVE FLUID TO CONTROL CIRCULATION LOSS

ESTUDOS REOLÓGICO E ESTATÍSTICO DE UM FLUIDO SENSÍVEL AO CISALHAMENTO PARA CONTROLAR PERDAS DE CIRCULAÇÃO

Dissertation presented to the School of Mechanical Engineering and Institute of Geosciences of the University of Campinas in partial fulfillment of the requirements for the degree of Master in Petroleum Sciences and Engineering in the area of Reservoirs and Management.

Dissertação apresentada à Faculdade de Engenharia Mecânica e Instituto de Geociências da Universidade Estadual de Campinas como parte dos requisitos exigidos para a obtenção do título de Mestre em Ciências e Engenharia de Petróleo na área de Reservatórios e Gestão.

Orientadora: Profa. Dra. Rosangela Barros Zanoni Lopes Moreno

Este exemplar corresponde à versão final da dissertação defendida pelo aluno George Hans Sterling Mora e orientada pela Profa. Dra. Rosangela Barros Zanoni Lopes Moreno.
.

CAMPINAS

2020

UNIVERSIDADE ESTADUAL DE CAMPINAS

FACULDADE DE ENGENHARIA MECÂNICA

E INSTITUTO DE GEOCIÊNCIAS

DISSERTAÇÃO DE MESTRADO ACADÊMICO

RHEOLOGICAL AND STATISTICAL STUDIES OF A SHEAR-SENSITIVE FLUID TO CONTROL CIRCULATION LOSS

ESTUDOS REOLÓGICO E ESTATÍSTICO DE UM FLUIDO SENSÍVEL AO CISALHAMENTO PARA CONTROLAR PERDAS DE CIRCULAÇÃO

Autor: George Hans Sterling Mora

Orientadora: Profa. Dra. Rosangela Barros Zanoni Lopes Moreno

A Banca Examinadora composta pelos membros abaixo aprovou esta dissertação:

Profa. Dra. Rosangela Barros Zanoni Lopes Moreno
Departamento de Energia / Faculdade de Engenharia Mecânica / Universidade Estadual de Campinas

Prof. Dr. Paulo Roberto Ribeiro
Departamento de Energia / Faculdade de Engenharia Mecânica / Universidade Estadual de Campinas

Rosana Fatima Teixeira Lomba
Programa de Engenharia Química/COPPE/Universidade Federal do Rio de Janeiro

A Ata da Qualificação com as respectivas assinaturas dos membros encontra-se no SIGA/Sistema de Fluxo de Dissertação e na Secretaria do Programa da Unidade.

Campinas, 16 de dezembro de 2020

DEDICATION

I dedicate this work to my dear parents, to my family with whom I can always trust, and who give me their support in every project that I start, and to my friends

ACKNOWLEDGEMENTS

"Um homem nunca deve sentir vergonha de admitir que errou, o que é apenas dizer, noutros termos, que hoje ele é mais inteligente do que era ontem"

Alexander Pope (1688-1744, poeta)

RESUMO

Palavras Chave: Perda de circulação, Fluido sensível ao cisalhamento, Fluido Dilatante, Tensão de escoamento, Desenho de Experimentos.

O pré-sal brasileiro, composto por carbonatos altamente fraturados, tem sido um enorme desafio para as operações de perfuração. Ao se perfurar carbonatos fraturados, o fluido de perfuração pode escoar para as fraturas ou cavernas, causando perda de circulação e, como consequência, controle ineficaz das pressões do fundo do poço. Este problema pode comprometer o poço e levar a um período não produtivo, custos associados a tratamentos para isolar a zona de perda e, às vezes, à perda total do poço perfurado. Existem métodos físicos e químicos ou uma combinação de ambos para o tratamento das perdas de fluido de perfuração. As soluções variam de acordo com a gravidade. Geralmente fluidos de perfuração customizados são suficientes para criar um filme denominado reboco na face do poço aberto, que previne a invasão do fluido de perfuração na rocha perfurada. Para perdas mais severas, são utilizados, lama de alta viscosidade, tampões de cimento, materiais de reticulação, gunk plug (óleo diesel-bentonita) e sistemas espessantes (também chamados de fluidos sensíveis ao cisalhamento, ou sistemas deformáveis-viscosos-coesivos).

Este trabalho visa estudar um fluido capaz de selar a zona de perdas, aproveitando suas propriedades visco-elásticas e sua capacidade de permanecer como um sólido enquanto tensões são impostas. Isso está diretamente relacionado com a tensão limite de escoamento. A metodologia consiste no estudo reológico de um material composto por olefina, bentonita, surfactante (Liomul), poliacrilamida (Flopaam 6030 S) e água destilada. São realizados testes oscilatórios de cisalhamento (testes de varredura de amplitude e testes de varredura de frequência) para encontrar a tensão limite de escoamento de cada formulação. Os testes foram desenvolvidos a 25 °C, utilizando-se o reômetro Thermo Scientific HAAKE MARS III equipado com geometria de placas paralelas (P35-Ti-L, com 0,8 mm de folga). Para cada formulação, a região viscoelástica linear (LVR) foi definida e a tensão limite de escoamento foi calculada. Análises estatísticas foram aplicadas, identificando-se a melhor formulação. Os resultados para todas as formulações mostram que o módulo elástico (G') ultrapassa o módulo viscoso (G'') para a região viscoelástica linear em 4 a 11 vezes.

A partir deste estudo, pode-se concluir que o material se comporta como um sólido se submetido a tensões menores do que a tensão limite de escoamento. A tensão limite de

escoamento do material é influenciada diretamente pelo teor de olefinas, e, finalmente, a formulação composta de nível baixo de olefina/bentonita (1 w%), nível baixo de agua/bentonita (2 w%), nível alto de polímero/bentonita (0,02 w%) e nível médio de tempo de agitação (90 s) é a formulação indicada para desenvolver testes de perda de circulação para avaliar as propriedades de vedação do material.

ABSTRACT

Key Words: Circulation loss, Shear-Sensitive Fluid, Thickening fluid, Yield Stress, Design of Experiment.

The Brazilian pre-salt is comprised of highly fractured carbonates and has been an enormous challenge for drilling operations. When carbonates are drilled, the drilling fluid can flow into the fractures or caverns, causing circulation loss and risking the well control. This problem can compromise the wellbore and leads to a non-productive time, over costs associated with treatments to isolate the thief zone, and sometimes the loss of the drilled well. There are physical and chemical methods or a combination of both for the treatments of drilling fluid loss. The solutions vary according to the severity. Generally, tailored drilling fluids are enough to create a filtered cake on the face of the open well, mitigating seepage losses. For more severe losses, high viscosity mud, cement plugs, crosslinking materials, gunk plugs (reverse diesel oil bentonite), thickening systems (also called shear-sensitive fluids or deformable-viscous-cohesive systems) are used.

This work aims to study a shear-sensitive fluid, able to seal the zone of loss, taking advantage of its viscoelastic properties and its ability to stay as a solid while stress is imposed. The methodology consists of rheological and statistical studies of a material composed of olefin, bentonite, surfactant (Liomul), polyacrylamide (Flopaam 6030 S), and distilled water. Oscillatory shear tests (amplitude sweep tests and frequency sweep tests) are performed to find the yield stress of the formulations. The tests were developed at 25 °C, using the Thermo Scientific HAAKE MARS III rheometer equipped with the parallel plates geometry (P35-Ti-L, with a gap of 0.8 mm). Statistical analyses were applied, and the best formulation was identified. The results for all formulations show that the elastic modulus (G') surpasses the viscous modulus (G'') for the linear viscoelastic region by 4 to 11 times.

From the study, it can be concluded that the material behaves like a solid when submitted to stress conditions lower than the yield stress. The olefin content directly influences the final yield stress of the material. Finally, with the statistical analyses, the best formulation was defined for a low level of Olefin/Clay (1 w%), low level of Water/Clay (2 w%), high level of Polymer/Clay (0.02 w%), and a medium level of stirring time (90 s). The optimized formulation is indicated to develop future tests for lost circulation, aiming to evaluate the sealing properties of the material.

LIST OF FIGURES

LIST OF TABLES

LIST OF NOMENCLATURES

Latin characters and expressions

A	-	Area	-	m^2
AV	-	Apparent Viscosity	-	$Centipoise$
B	-	Buoyancy	-	$-$
D	-	Diameter	-	m
DF	-	Degree of freedom	-	$-$
ECD	-	Equivalent Circulation Density	-	g/cc
e_f	-	Effect of parameter	-	$-$
F	-	Fisher number	-	$-$
G'	-	Elasticity (or storage) modulus of the material	-	$L^{-1}M^1T^{-2}\Theta^0N^0$
G''		Viscous (or loss) modulus of the material	-	$L^{-1}M^1T^{-2}\Theta^0N^0$
h	-	Thickness	-	m
K	-	Consistency index	-	$L^{-1}M^1T^{n-2}\Theta^0N^{0*}$
L	-	Length	-	m
MS	-	Medium Squares	-	$-$
MW	-	Mud weight	-	g/cc
n	-	Fluid flow behavior index	-	$-$
P	-	Pressure	-	psi
P_h	-	Hydrostatic pressure	-	psi
PV	-	Plastic Viscosity	-	$Centipoise$
p_w	-	Wetted perimeter	-	m
Q	-	Volumetric flow rate	-	m^3
r	-	Radius	-	m
R^2	-	Coefficient of determination	-	-
SS	-	Square sum	-	$L^0M^0T^0\Theta^0N^0$
S^2	-	Variance	-	$-$
V	-	Mean velocity of fluid	-	m/s
X	-	Generic variable	-	-
$\hat{y}$		Vector of responses	-	-
YP	-	Yield Point	-	$lb/100\,ft^3$

Greek characters

α	-	Significance level	-	$-$
$\dot{\gamma}$	-	Shear rate	-	s^{-1}
ε	-	Error	-	$-$
η	-	Apparent viscosity	-	$Centipoise$
μ	-	Viscosity	-	$Centipoise$
ρ	-	Specific mass	-	g/cc
τ	-	Shear stress	-	Pascal
ω	-	Angular velocity	-	$L^0M^0T^{-1}\Theta^0N^0$
μ_{eff}	-	Effective viscosity	-	$Centipoise$

Acronyms

API	-	American petroleum institute
HPAM	-	Partially hydrolyzed polyacrylamide
DOE		Design of Experiment

SUMMARY

1 INTRODUCTION

Operations to explore and develop oil and gas projects are complex, and the cost of searching for hydrocarbon reserves becomes more expensive when drilling occurs offshore, in deep water, and in hostile environments. Consequently, it is essential to control all steps of the involved operations, from the geological studies to the transport of the hydrocarbons to the refinery.

One factor that defines the success of the hole construction during drilling operations is the drilling fluid selection, characteristics, and behavior under specific conditions. This fluid cools the drill string, transports rock cuttings out of the well, prevents the surrounding formation from collapse, helps on the wellbore control, and prevents filtration of fluids into the rock formation (APALEKE; AL-MAJED; HOSSAIN, 2012).

The Brazilian pre-salt comprises highly fractured carbonates and has been an enormous challenge for drilling operations (PINHEIRO *et al.*, 2015). A common problem in this type of formation occurs when the drilling bit finds fractured zones, where the drilling fluid escapes from the hole. It means that the injected fluid does not return to the surface completely. The fluid flows into the formation at different flow rates, from filtration in permeable rocks to total losses in fractured carbonates, and the treatments vary according to the severity of the losses. Those circumstances cause other problems associated with underbalanced pressure, which can compromise the wellbore stability and wellbore control (ASTON *et al.*, 2004; LOMBA *et al.*, 2013)

The loss of circulation leads to millions of dollars of increased cost every year for petroleum exploration worldwide, and a non-efficiently controlled circulation fluid loss can result in losing the drilled well (ELKATATNY *et al.*, 2020; PINHEIRO *et al.*, 2015). Solutions to mitigate fluid loss can be classified according to the drilling fluid type and lost fluid flow rate. Oil-based fluid circulation loss is considered as seepage loss when the loss rate is minor than 10 bbl/h (1.6 m^3/h), a moderate loss for rates between 10 and 30 bbl/h (1.6 – 4.8 m^3/h), a severe loss for rate more than 30 bbl/h (>4.8 m^3/h); and total loss when there are no returns to surface. For seepage losses, the materials presented in the drilling fluids are enough to create a film called cake on the face of the open well. Treatments for moderated and severe losses start by using loss circulation materials (LCM, granular, foliated, or fibers). Total loss requires

treatment pills, which include high viscosity mud, cement plugs, crosslinking materials, resins, gunk plugs (reverse diesel oil bentonite), and thickening systems (also called shear-sensitive fluids, deformable-viscous-cohesive material) (AL-HAMEEDI *et al.*, 2018; ALKINANI *et al.*, 2019, 2020; HOSSAIN; ISLAM, 2018; RAHMAN, 2000; TEIXEIRA *et al.*, 2014).

The selected treatment should provide some characteristics to successfully seal the fractures and stay put for an extended period. The fluid needs to be pumpable from the surface to the bottom hole, and once positioned, it needs to present high yield stress to prevent its removal from the fractures and prevent any mud from passing through it. Moreover, that property is desirable at the thief zone (loss zone), not before, along the drill string (DATWANI, 2012). Materials that achieve the mentioned characteristics are the thickening fluids, named shear-sensitive fluids in this dissertation.

The shear-sensitive material focused on this study is a pumpable product that, due to their chemical and physical interactions, becomes almost solid when the shear forces exceed a critical value, strong enough to maintain its elastic behavior without altering in the zone of loss. The material is useful for non-reservoir zones for the difficulty to be removed.

1.1 Motivation

The interest to explore the Brazilian pre-salt located in deep and ultra-deep waters requires the use of technology and materials increasingly specialized in optimizing the wellbore drilling processes.

Circulation loss of drilling fluids is one of the most expensive problems that can occur during drilling operations. Synthetic fluids are excellent for drilling the salt. However, the loss of circulation is critical. Prepare this fluid at the platform is difficult, and in the case of severe loss, an extra amount of synthetic fluid must be brought from land, which is expensive.

The treatment fluid must remain stable during the time needed to finish each drilling section and to position the casing. Usually, solid materials are used to control this problem (also called LCM's that could be granular, foliated, or fibrous). According to the literature, when the LCM's and other methods fail to control the circulation loss, the solution is the use of high viscosity materials as crosslinked polymers or shear-sensitive fluids. However, there are some problems associated with these methods. The LCM's can plug the tools used in production

systems, while cement and crosslinked systems present a long setting time. On the other hand, thickening fluids act in less time compared with the other mentioned methods.

The motivation to study shear-sensitive materials (SSM) is because they use fewer resources (components) that are usually available in the platform, and they characterize by a short activation time, thickening properties, and high yield stress. The fluid is an easily pumpable liquid before it passes through the drill bit, where it thickens when it passes through the nozzles and is highly sheared by the applied forces. Therefore, the material can be placed in the thief zone in less time compared to other methods. Consequently, this type of fluid is an indicated candidate to be evaluated as a solution for the circulation loss problem.

1.2   Objectives

The present research focuses on the design, evaluation, and optimization of a shear-sensitive material composed of olefin, bentonite, surfactant, polyacrylamide, and water, which effectively decreases circulation loss in fractured carbonates.

The specific objectives to validate that are:

- Perform rheological characterization of the formulation and choose the most promising one, according to final yield stress.
- Evaluate the time interval of high shear mixing applied on the material as a factor that could affect the final yield stress
- Optimize a formulation to achieve the highest yield stress.

1.3   Dissertation organization

This dissertation is divided into six chapters.

Chapter two describes the fundamental concepts to understand the drilling process, the drilling fluids, and circulation loss. Additionally, a literature review related to shear-sensitive fluids is presented, where the properties of each material, laboratory tests, and field tests are analyzed. Some fundamentals of rheology are studied, and, finally, the bases of statistical analyses are presented to support the selection of the material.

Chapter three shows the methodology applied in this study, from the experimental design to the fluid evaluation, where a model that predicts the yield stress of the material is built.

Chapter four shows the results of the data collected with the methodology presented in the previous chapter to obtain the best shear-sensitive formulation composition.

Chapter five shows the main conclusions and recommendations for future works.

2   BACKGROUND AND LITERATURE REVIEW

This section discusses the importance of drilling fluids and problems related to circulation loss and possible solutions. Laboratory tests conducted for drilling fluid evaluation and loss control studies are also presented.

2.1   DRILLING OPERATIONS

Drilling a well is an operation designed to create a pathway from the surface to the reservoir. Simultaneous actions are executed to achieve the reservoir, such as breaks the rock into small particles using a drill bit, which is rotated and simultaneously forced against the rock at the bottom of the hole. Many drilling fluid functions can be mentioned, such as maintain the stability of the wellbore walls, prevent the fluids of the formations from entering into the well and avoid the uncontrolled invasion of the drilling fluids into the formation (HOSSAIN, 2016).

The drilling process is achieved by using drilling rigs (onshore and offshore). The essential equipment of a drilling rig consists of a structure that can support several hundred tons, the hoisting system, the rotary system, the circulation system, the power and prime movers, and well control components (AZAR; SAMUEL, 2007).

The equipment used on a platform-based operation (Figure 2.1) depends on where the drilling is conducted and what floating drilling vessel is selected (drillship or semi-submersible or a stable Jack-up vessel) (AZAR; SAMUEL, 2007).
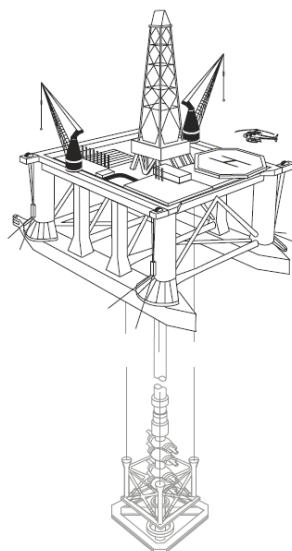
Figure 2.1 Semi-Submersible Drilling Rig. Source (AZAR; SAMUEL, 2007)

A drilling fluid designed according to the geological conditions is used to drill the well. The fluid is composed of an aqueous, non-aqueous, or aerated continuous phase, and this phase is complemented by additives that help improve the rheological properties of the fluid. The formulation can include thickening or thinning agents, pH modifiers, colloidal solids, surfactants, biocides, and polymers. One of the most critical problems during drilling is related to the uncontrolled flow of the drilling fluid into the formation (thief zone) caused by the presence of fractures or caverns and the differential pressure between the fluid inside the wellbore and the pore pressure formation (HOSSAIN; ISLAM, 2018). This uncontrolled invasive flow is known as circulation loss.

2.2 DRILLING FLUIDS

A drilling fluid is a mixture of components that produces a stable material, which improves the drilling process and maintains the drilling operation safety. This fluid can be designed specifically for each depth and rock that would interact with it. The next pages explain the main functions, properties, types, and selection of each drilling fluid.

The principal factors governing the drilling fluid selection are the characteristics and properties of the formation to be drilled, the quality and source of the water used in the fluid, and the ecological and environmental considerations (MITCHELL; MISKA, 2011).

Drilling fluids are categorized according to their continuous phase and composition (Figure 2.2); therefore, there are water-based fluids, oil-based fluids, and pneumatic (gas) fluids.
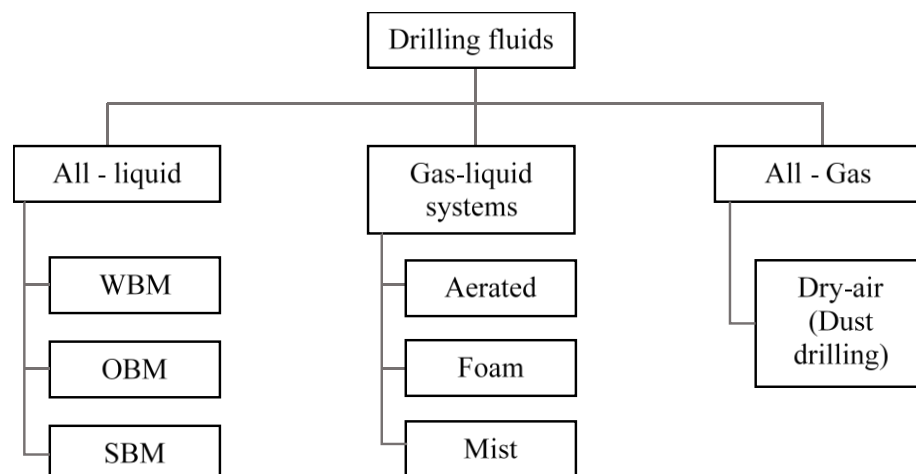
Figure 2.2 Classification of drilling fluids according to their composition. Source: (LAVROV, 2016)

Some of the essential functions of drilling fluids include controlling subsurface pressure, transport cuttings, stabilize the wellbore, and control the filtration (AMOCO PRODUCTION COMPANY, 1994).

During a drilling operation, the cuttings must be removed from the wellbore hole, and the fluid flowing from the bit needs to transport the material from the bottom to the surface; some factors that influence the capacity of the fluid to do this job are its velocity and viscosity (AMOCO PRODUCTION COMPANY, 1994).

Fluid invasion can occur in permeable formations. This problem can be controlled by the deposition of a filter cake (layer of concentrated solids from the drilling mud) on the formation face. That cake physically assists the stabilization of the formation (AMOCO PRODUCTION COMPANY, 1994).

Other functions of the drilling fluid include cooling and lubricate the bit, transmit hydraulic horsepower to the bit, provide a medium for wireline logging, minimize formation damage, reduce corrosion, minimize circulation loss, reduce stuck pipe, reduce pressure losses, improve penetration rates, reduce environmental impact and improve safety (ENERGY API, 2001).

Table 2.1 presents standard products used for the synthetic drilling fluids, their function, and the recommended proportion for each component.

Table 2.1 Products and proportions for Synthetic base fluid.

Product	Function	Unit	Proportion
Olefin	Dispersing phase	%Vol	60 -- 95
Water	Disperse phase	%Vol	05 -- 40
Lime	Rheologic stabilizer - pH	lb/bbl	4 --8
Liomul	Emulsifier	lb/bbl	9 -- 14
NaCl	Brine	%Vol aq.	15 -- 30
Organophilic clay	Viscosifier	lb/bbl	5 -- 8
Ecotrol	Filtrate controller	lb/bbl	1 -- 8
HRP	Rheologic modifier	lb/bbl	1 -- 2
Barite	Weight agent	lb/bbl	The necessary

Source: (AZAR; SAMUEL, 2007; NEFF; MCKELVIE; AYERS, 2000)
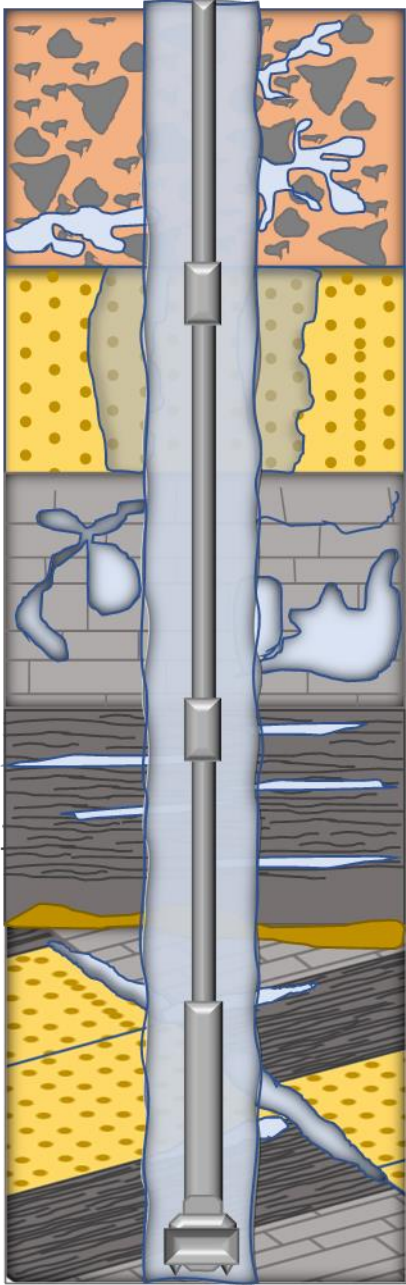
2.3 CIRCULATION LOSS

Circulation loss is an unexpected and uncontrolled flow of drilling mud into a formation. For loss of circulation to occur, there must be a high permeable formation or a

formation with flow channels that allow the fluid to pass from the wellbore to the formation driven by an overbalance differential pressure between the wellbore and the formation (MITCHELL; MISKA, 2011).

Table 2.2 shows the profile of a well that passes through several rock formations. The first column shows a geologic formation; the second column shows the type of formations and the characteristics correlated with the geologic formation section.

Table 2.2 Geological profile where circulation loss occurs

Geological profile	Characteristics
	Permeable zones: High primary porosity and permeability. They are presented in unconsolidated formations, gravel beds, loose conglomerates, and sandstones. It could be manifest as a gradual drop in the pit level. A total loss may happen if drilling continues.
	Cavernous: It is generally confined to limestone. The bit may drop from a few inches to several feet, just preceding the fluid loss. The loss of return may be sudden and complete.
	Induced fractures: They are related to drilling fluid or cementing programs and may occur in any type of rock. However, it is expected in shales. If the losses do not start in a wellbore, but in adjacent wells, one can suspect the occurrence of induced fractures.
	Natural fractures: It is related to secondary porosity and permeability (carbonates). Loss is evidenced by a gradual lowering of mud in pits. If drilling continues, more fractures may be exposed to complete loss.

Source: Adapted from: (AMOCO PRODUCTION COMPANY, 1994; CHILINGAR; VORABUTR, 1983; MITCHELL; MISKA, 2011).

Mud losses of synthetic base fluids can be classified according to their severity, as seepages (less than 10 bbl/h), common in sandstones, partial losses (10 to 30 bbl/h) found in unconsolidated sand or gravel with narrow fractures, severe losses (more than 30 bbl/h) associated to sand or gravel with more extensive fractures, and total losses (no returns to the surface) associated with vugular or cavernous formations, heavily fractured rocks, or systems with large fracture apertures (LAVROV, 2016).

The key to preventing induced lost circulation remains in controlling static and dynamic pressures at all times, keeping the sum of these imposed loads below the fracture limit of the rock that is being drilled (AMOCO PRODUCTION COMPANY, 1994). Another mitigation method is running an intermediate casing in the transition zone (ELKATATNY *et al.*, 2020).

2.4   TREATMENT FLUIDS

The present section aims to show a literature review carried out on treatment fluids to mitigate circulation loss, focusing on materials that use high viscosity and high yield stress as target properties to solve the problem. Once the treatment fluid is selected, the components used are identified, and their availability on the drilling platform is verified.

The selected treatment for circulation loss needs to provide some characteristics to successfully seal the fractures and maintain them sealed for an extended period. Therefore, a high yield stress value is required to prevent removing the material from the fractures and prevent any mud from passing through it (DATWANI, 2012). The material behaves as a solid below the yield stress, but when the critical stress is reached, the material yields to flow (viscoelastic behavior) (IRGENS, 2014).

When the loss starts, the better solution is creating a sealing material able to reduce the permeability of the zone; among the methods used, the following ones are included: crosslinking fluids (Caughron et al., 2002), gunk slurry (SHAHBAZI; NAZEMI, 2018) or shear-sensitive fluids (MABERRY; GARRISON; GARNIER, 2004).

Figure 2.3 provides a lost circulation strategy organized depending on the remedy efficiency (high probability of success); this is useful to maximize the treatment success and minimize non-productive time due to appropriate actions and corrective measures associated with more economical treatments.
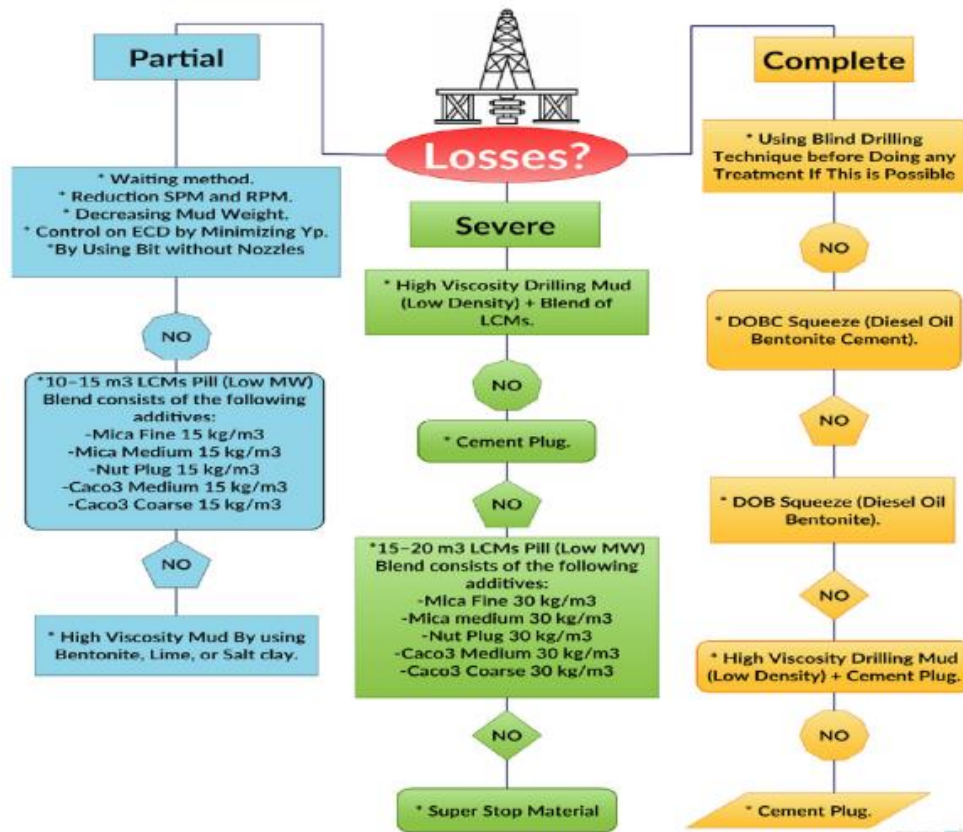
Figure 2.3 Treatment strategy to control circulation loss. Source: (AL-HAMEEDI et al., 2018)

2.4.1 Cross-linked Systems

Crosslinked Systems are based on the link between two chains of polymers and a crosslinked-agent that is activated by time, temperature, or shearing at the bit. After the activation, the treatment fluid turns into a rubbery, ductile, and stable material that seals the channels and prevent further losses (LAVROV, 2016).

The plugging efficiency can be evaluated with a particle plugging apparatus (PPA) described in the API RP 13I. It is an HPHT equipment that measures the bridging characteristics of the materials, where fractures width from 2 to 5 mm can be simulated, under pressures below 5000 psi (34.5 MPa) and temperature up to 500 °F (260 °C) (API RP 13I, 2000).

Ivan et al. (2002) developed a study of crosslinked polymer pills (PCP) to stop lost circulation on induced fractures. All these pills are activated by crosslinking agents, time and temperature, or by shearing at the bit. When set, they produce a substance described as rubbery, spongy, and ductile. A field trial was developed, where an induced fracture with a fracture height of 600 feet was sealed using 110 bbl of PCP; the highest yield stress of the pill was 2000 Pa after cross-linked, and, according to the authors, the results showed excellent control of the propagation of the induced fracture and reduction on drilling fluid loss.

A gel plugging material test (GMT) apparatus, composed of a plexiglass tube filled and packed with glass beads to imitate a thief zone, was used by Hashmat et al. (2016). Using this apparatus, they evaluated two systems, Polyacrylamide (HPAM)/Polyethyleneimine (PEI) (3/1.2) and A130/PEI (2/1.2), and they had successfully prevented mud loss in a zone of 300 D permeability at 25 °C (77 °F) and differential pressure of 150 psi (1034 kPa).

Song et al. (2018) found that a system composed of polyacrylamide (PAM) and PEI as a crosslinker, with a yield stress of 200 Pa, reduced around 95% of the permeability of 1544 mD in artificial cores (SONG; JIANG; WANG, 2018).

Jiang et al. (2019) used HPAM and methylene bisacrylamide (MBA) as a cross-linker and achieved a yield stress value of 1500 Pa. The material was evaluated using a gel plugging material test (GMT). Using a removable cylindrical iron with a 5 mm slot, they showed that the hole was sealed with success supporting up to 1000 psi of differential pressure (JIANG *et al.*, 2019).

2.4.2 Gunk slurries

The gunk slurries involve a gunk plug containing a large quantity of clay or hydratable polymer mixed into an oil phase. That mixture forms a sticky gunk when the downhole water interacts with the hydratable material, and then, the gunk can seal the formation. A typical gunk plug recipe is 350 lb of bentonite in 1 bbl of diesel oil (HOSSAIN; ISLAM, 2018; MINTZ; IRANI, 1983).

The patent of Verret (2015) proposed a method to decrease circulation loss during wellbore operations. The method consists of injecting two fluids; the first one is an aqueous fluid containing at least one expandable polymer in an alkaline environment. The second fluid contains a hardening composition to increase the pH in situ, forcing the polymers to absorb water. Therefore, when both fluids mix, the resultant fluid expands, sealing the lost circulation zone. A field application was tested in a well that suffered total circulation loss, where an LCM was pumped without success. The proposed pill was pumped; first 50 bbl of the hard water fluid followed by 3 bbl of the drilling fluid, and then 100 bbl of a water-polymer blend. After the setting time, the complete return of drilling fluid was recovered (VERRET, 2005).

Ryan et al. (2015) present a successful application of reverse gunk pill to cure losses in limestone, while using non-aqueous phase (NAF) as a drilling fluid. Organophilic clay was studied as hydratable material for the reverse gunk (175 lb/bbl), and a proportion of 1 (NAF):1

(Reverse gunk) presented the best hydration of the clay. Case study 1 presents total dynamic loss that was controlled using 80 bbl of reverse gunk.

Miranda et al. (2017) used an apparatus consisting of a glass pipe filled with glass spheres, with an external concentric pipe, where water in the desired temperature circulates. They studied a fluid composed of hydrated bentonite pellets as a bridging material. The system (430 kD of permeability and 100 psi of differential pressure) was pressurized during 1 h 30 min; when no flow was observed in the out valve, they considered that the ability of the bentonite as a plugging material was proved (MIRANDA *et al.*, 2017).

2.4.3 Shear sensitive fluids

Shear sensitive fluid (SSF) is a Non-Newtonian fluid in which colloidal materials are dispersed in the fluid. The viscosity of an SSF can increase dramatically to become almost a solid when the shear rate exceeds a critical stress value. For example, in the system of corn starch and water (GE *et al.*, 2017).

The patent of Mintz and Irani (1983) considered the shear strength as the parameter to be improved to seal and bridge the loss zone. Mintz and Irani named the studied material as shear thickening fluid. This fluid stays with low viscosity when pumped through the drill string, and once forced to pass by the nozzles of the drill bit, it experiences a high shear and sets up into a high viscosity, semi-rigid, and high strength paste. The material is composed of diesel oil, soluble oil surfactant, bentonite clay, polymer, and an aqueous phase. The surfactant is mixed with the oil to enhance its surface activity and stabilize the clay to prevent premature gelling under low shear mixing conditions. They used polyacrylamide as a hydratable polymer, which has three functions: to slow down hydration of the clay, help shape a high strength paste and make the composite more easily pumpable. The optimal composition with the higher strength reported in the patent was as surfactant/clay (0.24), oil/clay (0.49), and polymer/clay (0.033). That formulation achieved a shear strength of 19000 lbf/100 ft^2 (9100 Pa).

Hamburger et al. (1985) used the material developed by Mintz and Irani (1983) and run laboratory tests to prove its effectiveness in the field. The fluid system was composed of mineral oil (16.5 w%), polyamine oil-soluble surfactant (5,5 w%), Wyoming bentonite (29.3 w%), dry polyacrylamide polymer (1.0 %weight), and water (47.7 w%), achieving a strength of 6000 lbf/100 ft^2 (2880 Pa). The authors found that the slurry remained pumpable for 4 to 6 h because the water slowly diffused into the clay particles; this was visible by a simple

thickening-time test where a modified Fann viscosimeter was used to measure the time the fluid took to achieve 100 cP (10 Pa.s). In their case, it was 35 min. The field application presents a case where total returns were lost, and lost circulation material (LCM) pills were pumped without success, then 85 bbl of the shear thickening fluid was pumped between two spacers, successfully achieving the complete returns on the surface (HAMBURGER *et al.*, 1985).

Shaarpour (2004) studied a blend of lost circulation material with minimum solids and suggested the use of hydrogel (HPAM) as the main component to coat the expandable clays, as Mintz (1983) suggested. The material proposed by Shaarpour allows a more extended period to pump and circulate through mud motors. The material must be set in the lost circulation zones, including high permeability sandstones and limestones and small fractures, before it becomes a solid (SHAARPOUR, 2004).

Shahbazi and Nazemi (2018) presented a review of the selection of lost circulation materials for fractured oil reservoirs, and among other methods, they presented the shear-sensitive plugging fluids (SSPF). SSPF refers to a fluid that jellifies rapidly after passing through the bit, forming a solid mass that cures total mud loss. The SSPF consists of a shear-sensitive invert emulsion with a degree of instability to high shear forces; this is used to create a material resultant from the crosslinker encapsulation in the continuous oil medium, helped by surfactant and a water-soluble polymer in the water phase. A pressure drop more significant than 400 psi across a small orifice (drill bit nozzles) is necessary to rupture the emulsion and initiate the reaction, finally plugging the zone of loss.

Table 2.3 shows some characteristics of downhole motors to give an idea of the rate that fluids can flow through the drill bit nozzles. The shear stress that the fluids can achieve in the nozzles is 50 – 100 bar, and the shear rate ranges from 2000 to 10^6 s^{-1} (DRAKE; CALCAVECCHIO, 1987; SUNDE; KONRAD, 1986).

Table 2.3 Downhole motors

Diameter of the motor (in)	Configuration	Flow rate (gpm)	Velocity (rpm)	Type of velocity
4.75	2:3	100 - 265	200 - 550	High
4.75	7:8	150 - 250	30 - 75	Low
6.25	7:8	200 - 600	34 – 102	Low

Source: (BASSANTE, 2012)

Table 2.4 summarizes the review focused on materials capable of generating high viscosity and high yield stress. The third column shows the highest yield stress value reached

during the experiments of each author, the fourth column reports the overall composition of the fluid, the fifth column shows the properties of the rock or the formation in which the tests were performed, and the results reached in each test are presented the last column.

Table 2.4 Review of the methods and materials free of LCM for loss circulation control

Year	Author	Highest yield stress, Pa	Composition	Filtration medium	Result
1983	Mintz and Irani	9000	Oil (S100N), surfactant (Paranox 106), Clay bentonite, Polymer (P-250),Water	-	Not filtration test
1985	Hamburger et al.	2874	Mineral oil, Surfactant (Polyamine oil-soluble), Water, Polymer (Polyacrylamide), clay (Wyoming bentonite).	A field test with total losses	Successfully sealed
2002	Ivan et al.	5500	Blend of polymers and cross-linking agents	Induced fracture height 600 ft and 9 mm of width	Successfully plugged
2004	Shaarpour	Not measured	Wyoming bentonite, polyanionic cellulose, water, Soluble gum, water-soluble polymeric thickener	-	Show the use of the mixture polymer-clay as a controller
2005	Verret	Not measured	Chitosan, sulfaminic acid, super absorbent polymer, barite, micronized cellulose.	Total losses	Complete circulation returns
2015	Ryan et al.	Not measured	Organophilic clay, water, lignosulfonate, non-aqueous phase	Total Dynamic losses	Reported successful in building integrity
2016	Hashmat	Not measured	HPAM, PEI	300 D	Blocked the zone under a differential pressure of 150 psi
2017	Miranda et al.	Not measured	Bentonite Pellets	430 kD	Remediate severe loss circulation under a differential pressure of 100 psi
2018	Song et al.	200	Polyacrylamide (HPAM), Polyethyleneimine (PEI)	1544 mD	95% of permeability reduction
2018	Shahbazi and Nazemi	-	Encapsulation of the crosslinker in the continuous oil medium and a water-soluble polymer in the water phase	-	Show the theory of the use of shear sensitive plugging fluids
2019	Jiang et al.	1500	Cross-linker N′-Methylenebisacrylamide (MBA), monomer acrylamide (AM) and partial hydrolysis polyacrylamide (PHPA)	Cylindrical iron slot (50*40*3 mm)	Total sealing

From the presented literature, it was concluded that bentonite and polyacrylamide as thickening agents had been used successfully to solve circulation loss problems, and the use of shear-sensitive fluids has been proved to solve total circulation losses when the use of LCM's has not succeeded.

2.5 FLUID RHEOLOGY

Rheology is the study of the flow and deformation of matter. It is a physics and physical chemistry branch since the essential variables come from mechanics: forces, deflections, and velocities. It is critical to remember that it is impossible to measure, increase, decrease, or optimize rheology; instead, we can do this to viscosity or rheological properties (MEZGER, 2014). This chapter briefly presents the necessary rheological concepts for the development of this work.

The characterization of the physical properties of both drilling and loss control fluids is evaluated considering rheological studies. The fluids are classified as Newtonian or non-Newtonian. The viscosity of Newtonian fluids is independent of the applied shear. Non-Newtonian fluids viscosity depends on the shear rate, and they can be thickening or thinning fluids. Non-Newtonian flow behavior can be analyzed by varying the applied shear stress and measuring the shear rate. Flow curves data can be fit to particular models to represent the behavior of each material.

Figure 2.4 shows the conventional rheological models for Newtonian and non-Newtonian fluids and their equations in a plot of shear stress versus shear rate.

	Bingham	$\tau = \tau_0 \pm K \dot{\gamma}$
	Hershel-Bulkley	$\tau = \tau_0 + K \dot{\gamma}^n; \; n < 1$
	Ostwald-de Waele (Dilatant)	$\tau = K \dot{\gamma}^n; \; n > 1$
	Newtonian	$\tau = \mu \dot{\gamma}$
	Ostwald-de Waele (Pseudoplastic)	$\tau = K \dot{\gamma}^n; \; n < 1$

Shear Stress τ (Pa)
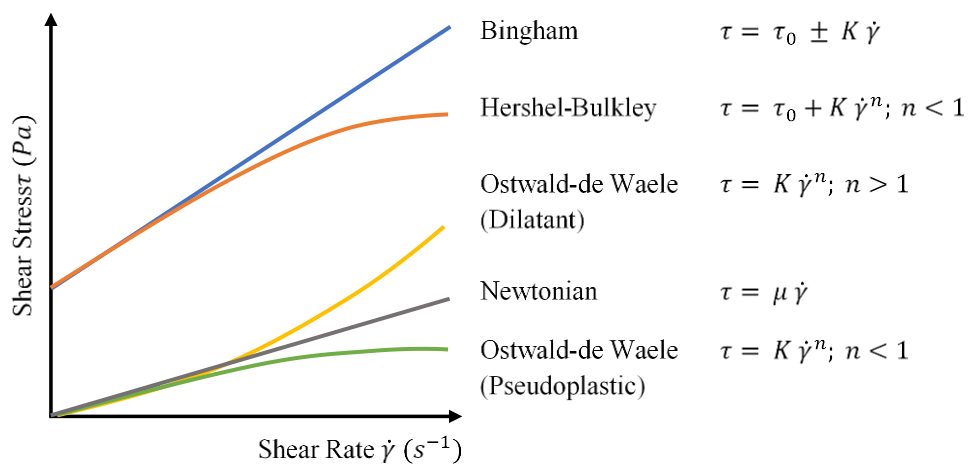
Shear Rate $\dot{\gamma}$ (s^{-1})

Figure 2.4 Flow curves

Where n is the flow behavior index, $\dot{\gamma}$ correspond to shear rate (s^{-1}), K is the consistency index (Pa.s^{n}), μ is the Dynamic viscosity (Pa.s), τ_0 are the yield stress (Pa), and τ is the shear stress (Pa) (MEZGER, 2014).

Many configurations can be used to measure fluid viscosity. Figure 2.5 shows the two-plates configuration, which is used to define fundamental rheological parameters. The upper plate with the area (A) is set in motion by the (shear) force F, and the resulting velocity v is measured. A distance h separates the plates, and the lower plate is stationary ($v = 0$). The sample is sheared in this gap. The following shear conditions are assumed to occur. The sample shows adhesion to both plates without any wall-slip effects, and the fluid flows under laminar flow conditions.
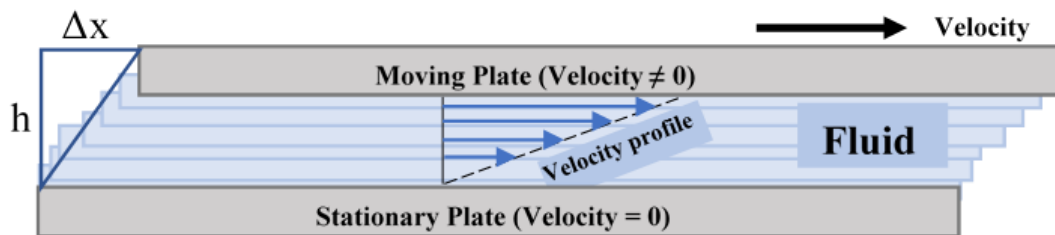
Figure 2.5 Concept of the velocity gradient. Source: Author

The Strain (γ), also known as shear strain, deformation or shear deformation, is the ratio between the change in length in one direction to the change in length in the perpendicular direction (Δx / h), see Figure 2.5.

The Shear Stress (τ) is the force required to sustain a fluid flow; see equation (2.1). In laminar flow, shear stress is the frictional drag existing between individual laminae (Figure 2.5). This is expressed as lbf/100 ft^2, or as Dyn/cm^2 (1 Dyn/cm^2 = 4.79 lb/100 ft^2), or as N/m^2 (1 N/m^2 = 10 Dyn/cm^2).

$$\tau = \frac{F}{A} \tag{2.1}$$

The Shear Rate ($\dot{\gamma}$) is the relative velocity of one plate moving by an adjacent plate (Figure 2.5), divided by the distance between them (equation (2.2)). That is expressed in s^{-1} (AMOCO PRODUCTION COMPANY, 1994).

$$\dot{\gamma} = \frac{v}{h} \tag{2.2}$$

The dynamic viscosity (μ) is the representation of a fluid's internal resistance to flow (equation (2.3)), defined as the ratio between shear stress and shear rate. Viscosity is expressed in poise, poise is a considerable number, and therefore, viscosity is typically reported in centipoise (100 centipoises = 1 poise = 0.1 Pa.s). Non-Newtonian fluids do not follow the linear law; therefore, an apparent viscosity (η) is introduced instead of the dynamic viscosity. Most of the drilling fluids are non-Newtonian (MITCHELL; MISKA, 2011).

$$\mu = \frac{\tau}{\dot{\gamma}} \tag{2.3}$$

Where τ (force/area) is the shear stress, $\dot{\gamma}$ (shear stress/time) is the shear rate, and μ is the viscosity (centipoise).

The rheological properties of the materials (qualitative and quantitative relationships between stresses and strains and their derivatives), for this study, were determined using a rheometer and a plate-plate geometry (Figure 2.6). That can be used for high viscous materials and when working on thermosetting or crosslinking materials.
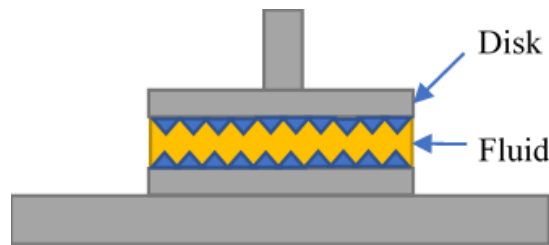
Figure 2.6 Geometry plate-plate

In parallel plate geometry (Figure 2.6), the shear deformation is maximum at the plate edge and zero at the center, so the shear rate is not uniform at all points in the material, and as a consequence, one has to check carefully if the amplitude of the input motion is small enough to verify the linearity hypothesis (COLLYER; CLEGG, 1988).

One of the considerations is to avoid the wall slip effect related to the space between the plates when using them to perform the rheological measurements (BUSCALL; MCGOWAN; MORTON-JONES, 1993; LARSON, 1999; ROY; AUDUS; MIGLER, 2019). It depends on the particles size. Commonly the gap used is around ten times the size of the bigger particle (ROMERO-ZERON; MANALO; KANTZAS, 2004). That length is used to find the optimum gap between the plate-plate geometry.

Oscillatory analyses can be used to obtain more complete rheological information about a material. By varying the frequency of disturbance, it is possible to obtain the mechanical spectrum of the material, where elastic and viscous contributions are observed as a function of the frequency of mechanical disturbance (See Figure 2.7).
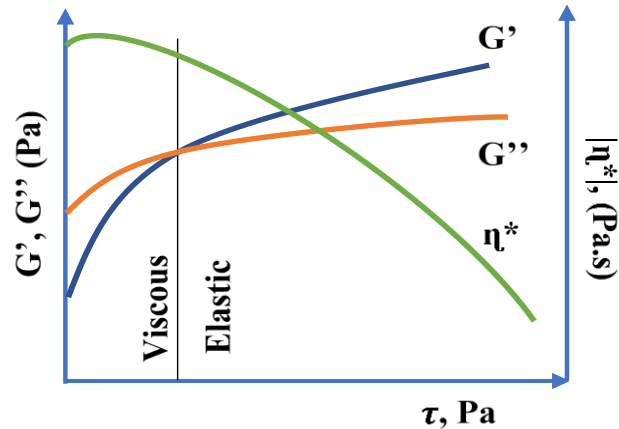
Figure 2.7 Viscoelastic flow properties

With the tests are identified the $\hat{G}$ is total complex modulus, this is the interaction between two modulus, the modulus G' (elastic modulus) defined in equation (2.5) and G'' (viscous modulus) equation (2.6), $\tan(\theta)$ that is the lag angle tangent (equation (2.7)), $|G^*(\omega)|$ the complex modulus that is the amplitude of deformation (equation (2.8)), and $|\eta^*(\omega)|$ that is the complex viscosity (equation (2.12)) (CLINCKSPOOR, 2019; KRISTENSEN, 2013).

$$\hat{G} = G' + iG'' \tag{2.4}$$

$$G' = \frac{\sigma_0}{\gamma_0}\cos(\theta) \tag{2.5}$$

$$G'' = \frac{\sigma_0}{\gamma_0}sen(\theta) \tag{2.6}$$

$$\tan(\theta) = \gamma(t)/\sin(\omega t) \tag{2.7}$$

$$|G^*(\omega)| = \frac{\sigma_0}{\gamma_0} = \sqrt{(G')^2 + (G'')^2} \tag{2.8}$$

$$|\eta^*(\omega)| = |G^*(\omega)|/\omega \tag{2.9}$$

Small amplitude oscillatory shear tests are used to characterize the fluid viscoelasticity (HYUN *et al.*, 2002). The viscoelasticity test includes an amplitude sweep test, which is performed by increasing the tension for a constant frequency to find the linear viscoelastic region (LVR) (KRISTENSEN, 2013). After that, the viscoelastic property of the long-term dispersion and the storage stability are evaluated by running a frequency sweep test.

Those tests aim to examine time-dependent deformation and indicate how long a fluid can stay uniform and stable under static conditions (GE *et al.*, 2017).

The Oscillatory Frequency Sweep Test consists of applying a frequency that increases controllably at constant stress. This test allows examining time-dependent deformation where the properties G', G'' stay stable. Long term behavior is simulated by low frequency and short term by high frequencies. In other words, the result is an indicator of the capacity of the fluid to suspend particles under static conditions (KRISTENSEN, 2013)(CLINCKSPOOR, 2019).

The Amplitude Sweep Test consists of selecting a constant frequency and analyzing how the elastic or storage module G' and the viscous or loss module G'' vary with the application of sinusoidal amplitudes over time (Figure 2.8).

This test allows finding the LVR that is characterized by the linear dependence between tension and deformation. In this region, the modules remain constant (Figure 2.8).

Fluids containing bentonite or polymers show a higher value of G' compared to G'' within the LVR range, proving gel-like behavior (Figure 2.8). The elastic portion dominates the viscous one, indicating specific stability in the low shear range (KRISTENSEN, 2013; RIBEIRO, 2017; ROMERO-ZERON; MANALO; KANTZAS, 2004).
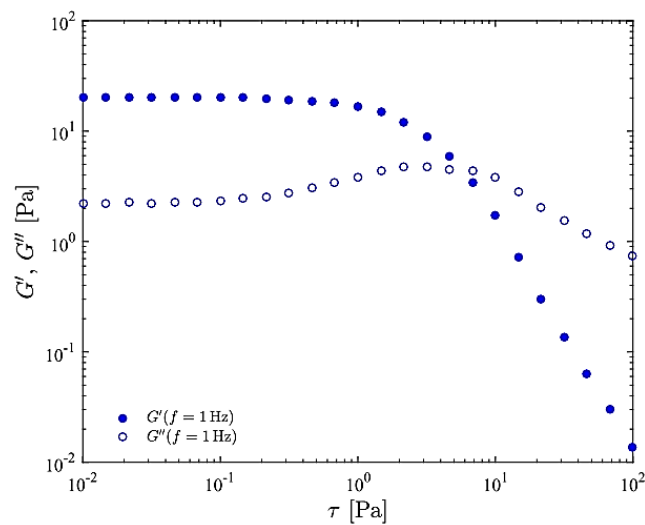
Figure 2.8 Amplitude Sweep Test of Carbopol® aqueous solution with glycerin. Source: (RIBEIRO, 2017)

The data analysis requires to find the region of linear viscoelasticity for the oscillatory segments. Besides, care must be taken with the presence of turbulent flow or

materials that settle quickly because that can generate erroneous readings of the analyzed properties (RIBEIRO, 2017)

The frequency sweep time is run by selecting a constant frequency and a constant amplitude, where the behavior of G' and G'' is observed over time (see Figure 2.9). This test is used to determine the viscous or elastic flow zones and the maximum time for reliable rheological analyses (RIBEIRO, 2017).

The oscillatory shear tests allow us to determine the yield stress, one of the properties of interest in the present work.
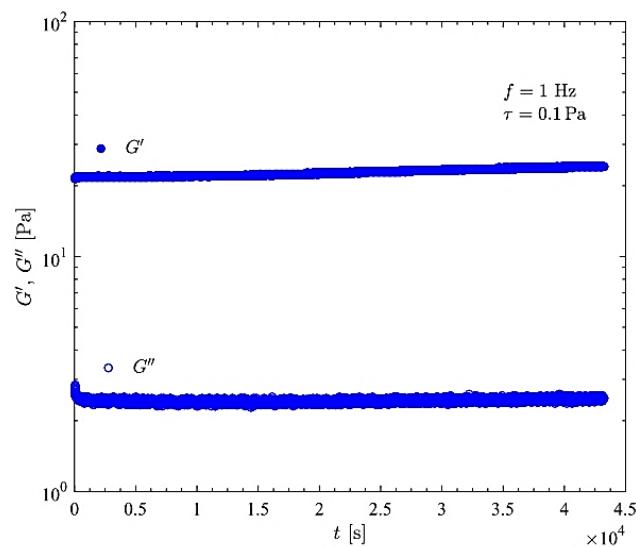
Figure 2.9 Frequency sweep time. Source: (RIBEIRO, 2017)

The yield stress can be determined by the controlled shear rate (CSR) method. However, since the yield point is dependent on the speedy resolution of the rheometer, its value is not directly determined. Therefore, existing models, such as Bingham, Casson, or Herschel/Bulkley, can be used to fit the measured data and then determine the yield stress value. These models produce different values for the yield point caused by the difference in the calculation basis (see Figure 2.10a). Plotting shear stress *versus* deformation (Figure 2.10b) and taking a straight line to fit the curve slope corresponding to the low-stress interval, the value, previous to the first inflection, corresponds to the searched point. In this initial interval, the fluid shows linear-elastic deformation behavior. According to the tangent crossover method, drawing two tangent fitting lines to the curve for shear stress *versus* deformation, one from the low shear stress and the second from the higher shear stress values, the yield point shear can be taken at the crossover point between the two lines (Figure 2.10c).

Following the DIN 51810-2 norm and taking the average value on the LVR (Figure 2.10d), the yield stress is given by a difference of 10% of that result (DEUTSCHES INSTITUT FUR NORMUNG E.V, 2011). According to the elastic stress method, the yield stress is denoted by the maximum in the elastic stress plot (elastic modulus (Pascals) *versus* shear strain (%)), see Figure 2.10e (WALLS *et al.*, 2003).
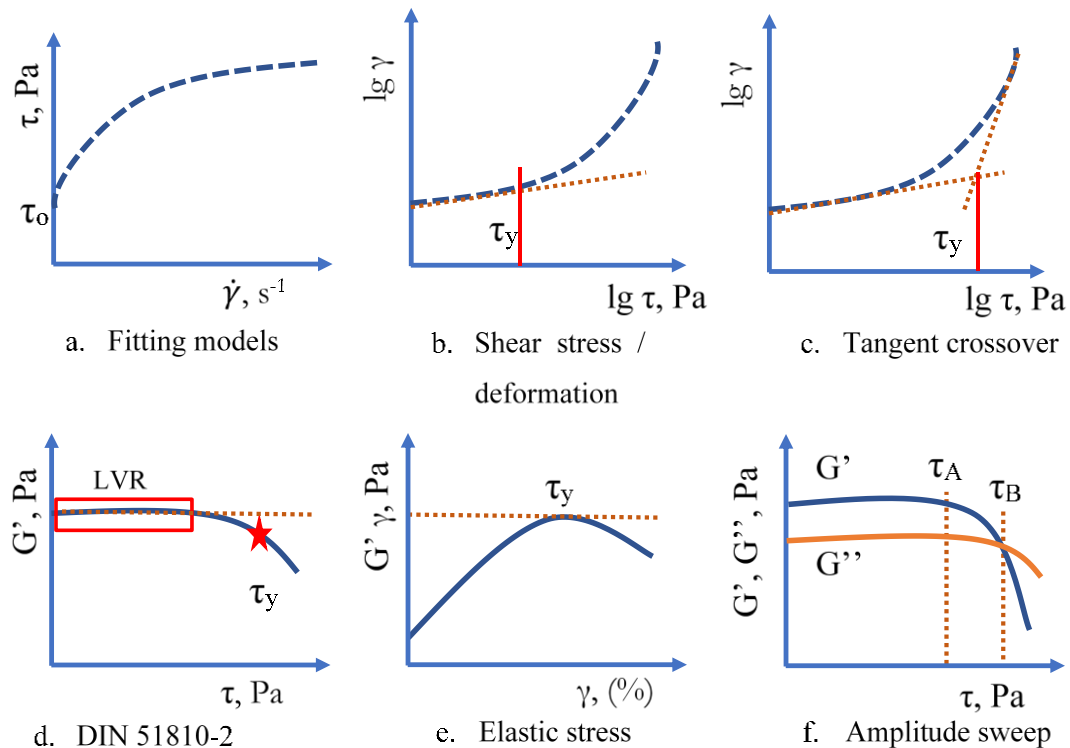
Figure 2.10 Yield point methods

Finally, the method applied for the amplitude sweep test analyses uses the limiting value of the LVR range in terms of the shear stress as the yield stress or the yield point (Figure 2.10f). No significant change of the internal structure occurs if stress values fall below the applied yield point; therefore, no yielding behavior can be observed in this range.

Once the rheological properties of the fluid are studied, a static filtration test could be developed to define what formulation suffers less filtration, for that is recommended to use a High temperature / High-pressure filter press. That is used as a cell capable of maintaining the working pressure as a maximum of 5000 psi (34.5 MPa) and a maximum temperature of 500 °F (260 °C), and a heating system. The use of ceramic cores is recommendable for testing (CAENN; DARLEY; GRAY, 2017).

Table 2.5 shows the behavior of shear rate along the drill string and some useful conversions.

Table 2.5 Shear rates in the circulating system and conversions

Source	In drill string	In equivalent rotational viscosimeter or Mixer
DP	100 – 500 s-1	60 – 294 RPM
DC	700 – 3000 s-1	410 – 1760 RPM
Bit Nozzles	10000 – 100000 s-1	5870 – 58700 RPM
Annulus	10 – 500 s-1	6 – 294 RPM
Mud pits	1 – 5 s-1	0,6 – 3 RPM
1° dial =	1.067 lbf/100ft2	5.109 dynes/cm2 Shear stress
1 RPM =	1.703 s-1 shear rate	1 Pa = 10 dynes/cm2
	1 PSI = 6894,8 Pa	1 dynes/cm2 =1/4.79 lbf/100ft2
	1 Pa.s = 10 Poise	

Source: (AMOCO PRODUCTION COMPANY, 1994)

2.6 DESIGN OF EXPERIMENTS (DOE)

The design of experiments (DOE) is the proper way to plan, run, and evaluate complex problems. In this, the tests to develop are determined, and, according to the method used, useful data are obtained to make the statistical analyses. According to Pulido and Salazar (2012), some typical problems that can be solved using DOE are, for example, compare two or more products to select the better one, determine the factors of a process that has an essential impact on the final product, find optimal conditions (e.g., temperature, humidity, or pH) to reduce the defects or improve a process, or make a process robust to fluctuations of environmental variables.

The definition of some concepts is essential to understand better the DOE. The characteristic of interest to be studied is called the response; the variables that influence the response are known as the factors; each factor can take different values called levels. The objective of the researcher is to describe the influence of the factors and his levels on the response (Figure 2.11) (NETO; SCARMINIO; BRUNS, 2001).
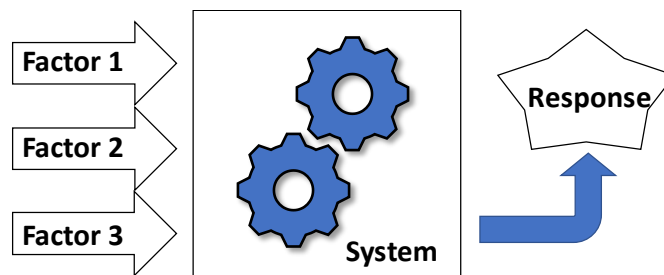
Figure 2.11 Factors and response in a DOE

The great variety of problems to be solved requires diverse experimental designs, and it is necessary to know the options to make the most efficient and straightforward process,

using the minimum of resources (materials, costs, time). Table 2.6 shows the classification of experimental designs, where the factorial design represents the most used and the most robust to analyze and optimize the data from experiments.

Table 2.6 Classification of experimental designs

Design	Types
Design to compare two or more treatments	Completely randomized design Random full block design Latin and Greco-Latin design
Designs to study the effect of the factors on one or more response variables	Factorial design 2k Factorial design 3k Fractional factorial designs 2k-p Nested designs Split-Plot Design
Design to process optimization	First-order model design Second-order model design
Robust design	Orthogonal Arrangements (factorial designs) Design with internal and external arrangements
Mixtures design	Simplex-reticular design Simplex design with centroid Axial design

Source: adapted from (PULIDO; SALAZAR, 2012)

The definition of the statistical hypothesis is necessary to develop a DOE. It is a statement of the process which is tested using the information of a representative sample. For example, a new design of drill bit can drill hard rock with 10% more efficiency than the older version.

H_0: p = 0.1 (the proportion is equal to 0.1)

H_A: p > 0.1 (the proportion is more than 0.1)

where H_0 is known as the null hypothesis, and H_A is the alternative hypothesis. Now, the objective is to prove the null hypothesis. In the example (Figure 2.12), H_A is known as the alternative hypothesis of one-way. Therefore, the alternative hypothesis is unilateral and depends on the affirmation to be proved (PULIDO; SALAZAR, 2012).
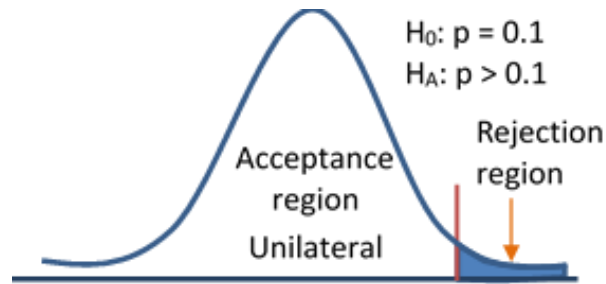
Figure 2.12 Hypothesis test, rejection and acceptance region

There is the risk of fall into an acceptance or rejection error of the hypothesis. Error type I occurs when the *Ho* is true, however, it is rejected, and error type II is when the *Ho* is accepted, however, it is false. The α value is the test significance and is the probability of the rejection region; the researcher defines this value, usually used as 0.05 or 0.01. That value means that more data is required to reject *Ho*. The p-value is known as the observed significance and corresponds to the area under the reference distribution; it is related to the Fisher value and the t-student distribution. The *p-value* needs to be less than α to reject *Ho* (PULIDO; SALAZAR, 2012).

The analysis of experimental data is developed by analyzing variance (ANOVA) (Figure 2.13). The general idea of this technique is to separate the total variation into parts that each source of variation contributes to the experiment (PULIDO; SALAZAR, 2012).
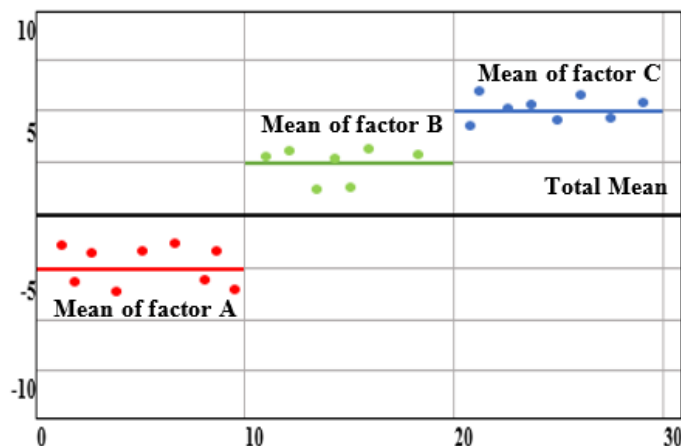
Figure 2.13 Representation of the means of effects and groups for ANOVA

Two of the most useful statistics to measure the overall quality of the model are the coefficient of determination (R^2) and the adjusted coefficient of determination (Adj R^2), which are obtained from the ANOVA. R^2 coefficient (equation (2.10)) measures the proportion of the total variability explained by the model and the total variability; it always increases when factors are added to the model, even when these factors are not significant. The adjusted R^2 statistic (equation (2.11)) is adjusted for the size of the model; it means that if non-significant

terms are added to the model, its value decreases (PULIDO; SALAZAR, 2012). R^2 values of 0.67, 0.33, and 0.19 in linear models are considered as substantial, moderate, and weak, respectively (HENSELER; RINGLE; SINKOVICS, 2009).

The R^2 predicted statistic indicates the fitting of the model and the prediction of future values. Equation (2.12) shows how to calculate the R^2 where the PRESS statistic is a measure of how well the model predicts new data (PRESS is the sum of squares of the prediction error) (MONTGOMERY, 2004).

$$R^2 = \frac{SS_{Model}}{SS_{Total}} \tag{2.10}$$

$$Adj\ R^2 = 1 - \frac{MS_{Error}}{MS_{Total}} \tag{2.11}$$

$$Pred\ R^2 = 1 - \frac{PRESS}{SS_{Total}} \tag{2.12}$$

A factorial design aims to study the effect of several factors on a specific response when all factors have the same interest. The factors may be qualitative, such as machines, the presence of a previous operation, or quantitative, such as pressure, the quantity of a specific material. It is necessary to choose at least two test levels to study how each factor influences the response. With the complete factorial design, all the possible combinations that can be formed with the levels of the factors to be investigated are randomly run. If there are two factors, but now one has three levels and the other two, 3×2 combinations can be built, resulting in the 3×2 factorial design. If the k-factors do not have the same number of levels, the product must be written explicitly; for example, with k = 3 factors, the first with three levels and the remaining two with two levels, then there is the factorial design $3 \times 2 \times 2$ or 3×2^2 (PULIDO; SALAZAR, 2012).

3 METHODOLOGY

This chapter presents the experimental design to analyze the factors and their levels that influence the yield stress given by a treatment fluid to control circulation loss. The preparation of the samples is detailed, as well as the statistical evaluation of the results. The primary goal is to identify the most significant component of the proposed formulation.

First, the experimental design was chosen. The selection was focused on understanding the influence of each component of the formulation on the response (yield stress) and then selecting the best formulation using an optimization process (see Item 3.6) (Figure 3.1).
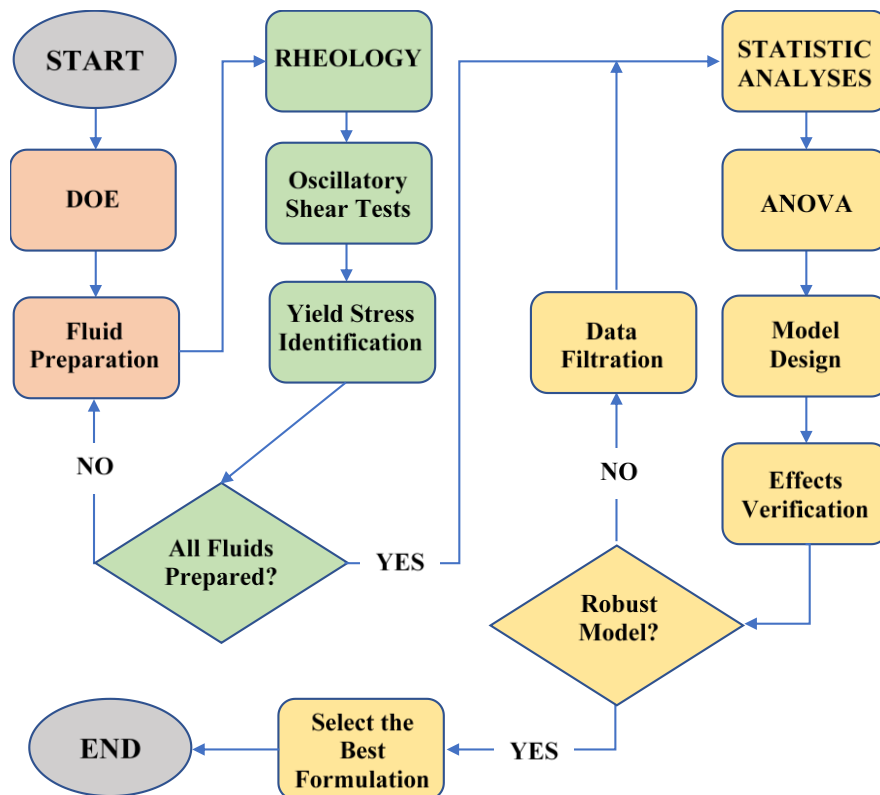

Figure 3.1 Workflow of Methodology for this work

3.1 Problem description and experimental design process

The study is focused on the control of high circulation loss in fractured carbonates while drilling using a synthetic base mud. Synthetic based drilling fluids were developed as an environmentally friendly alternative to the oil-based ones since they have similar mechanical

properties such as stability at high temperatures, high lubricity, and wellbore stability (MARQUES *et al.*, 2017), and has been the first choice to drill through evaporite sections in Pre-Salt zones, where circulation loss is a huge problem due to the costs of the drilling fluid and treatments to solve the problem (LOMBA *et al.*, 2013). Different treatments have been used, and viscoelastic materials are studied in this work as a solution for the losses.

The proposed viscoelastic material is a shear-sensitive fluid. When a high shear is applied to this material, it transforms into another fluid with higher yield stress. The high yield stress helps to improve the sealing properties of the fluids because the material stays as a solid into the fracture while this stress is not surpassed. Therefore, mud circulation loss decreases or stops.

The materials used to design the shear-sensitive fluid were Linear olefin (O), surfactant, bentonite clay, polyacrylamide, and deionized-distilled water (W), as suggested by Mintz and Irani (1983). The characteristics of some of the components are discussed in Appendix A.

Linear olefin is a synthetic liquid hydrocarbon obtained by polymerizing ethylene. For this work, the role of olefin is to maintain the clay particles in suspension, and this is achieved thanks to a dispersion of clay in oil/surfactant. The surfactant (Liomul NT) is a commercial product synthesized from amides and imidazolines; its function is to facilitate the suspension of the colloidal particles of clay on the olefin (AMORIM, 2017). Bentonite is an absorbent aluminum phyllosilicate clay consisting mostly of colloidal particles of montmorillonite, with a high capacity of swelling by contact with water (LAGALY; ZIESMER, 2003; XIE *et al.*, 2004). Polyacrylamide (HPAM) is highly water-absorbent, which turns into a soft gel when hydrated. The polyacrylamide used in this work was Flopaam 6030S (MW 20-22 million Daltons, degree of hydrolysis 40%, type post-hydrolyzed) (HASHMAT *et al.*, 2016).

The polyacrylamide retains water molecules until high shear stress is applied. The olefin phase acts as a barrier between the bentonite and water, but this can be ruptured by applying high shear. Water hydrates the bentonite, causing it to swell considerably, and makes the fluid solid-like. Polyacrylamide acts as a stabilizer of this final product, which not flows unless stress is applied. Distilled and deionized water was used to avoid unwanted chemical reactions with the reagents used in the formulation.

Since bentonite clay has significant importance on the formulation as seen before, it is convenient to express the concentration of the other components as a function of the bentonite and then decrease the factors. This way, the relation of the components with the bentonite is considered as the factors of the experiment and are expressed as follows: surfactant/clay (S/C), oil/clay (O/C), water/clay (W/C), and polymer/clay (P/C). Another factor of the study is the stirring time (T), which influences the final yield stress of the shear-sensitive fluid.

After the problem statement, variables of the study, and response selection, the levels for each variable need to be defined. Table 3.1 summarizes the studied variables and their corresponding levels. The levels were selected as the best one among the formulations presented for the patent of Mintz and Irani (1983), for the stirring time were selected the levels after previous tests, where the material was submitted to a different time of stir. The shear-sensitive material at 30, 90, and 150 s present visual differences on the texture and are selected as the range of stir time to be studied.

Table 3.1 Variables and correspondent levels of the experimental design

Factors	Low Level	Means Level	High Level
S/C (w%)	0.2	-	-
O/C (w%)	1.0	-	2.0
W/C (w%)	2.0	-	6.0
P/C (w%)	0.01	-	0.02
Stirring Time (s)	30	90	150

Once the factors and the individual levels are defined, the next step is to create the experimental design, that in our case, corresponds to a general full factorial design as presented in Chapter 2 - Item 2.7. The design of the experiment (DOE) of this study is shown in the next section.

3.2 Planning of the experimental work

The tests to be run along this work were planned according to a full factorial design of $2 \times 2 \times 2 \times 3$, including the following four factors (O/C, W/C, P/C, and T) and their respective levels. Table 3.2 shows the design of the formulations based on the levels defined before.

Table 3.2 General full factorial design

Formulation	Sample	O/C (w%)	W/C (w%)	P/C (w%)	Time (s)
	1	1.0	2.0	0.01	30
1	2	1.0	2.0	0.01	90
	3	1.0	2.0	0.01	150
	4	1.0	2.0	0.02	30
2	5	1.0	2.0	0.02	90
	6	1.0	2.0	0.02	150
	7	1.0	6.0	0.01	30
3	8	1.0	6.0	0.01	90
	9	1.0	6.0	0.01	150
	10	1.0	6.0	0.02	30
4	11	1.0	6.0	0.02	90
	12	1.0	6.0	0.02	150
	13	2.0	2.0	0.01	30
5	14	2.0	2.0	0.01	90
	15	2.0	2.0	0.01	150
	16	2.0	2.0	0.02	30
6	17	2.0	2.0	0.02	90
	18	2.0	2.0	0.02	150
	19	2.0	6.0	0.01	30
7	20	2.0	6.0	0.01	90
	21	2.0	6.0	0.01	150
	22	2.0	6.0	0.02	30
8	22	2.0	6.0	0.02	90
	24	2.0	6.0	0.02	150

For the next sections, the factors were renamed as follows: S/C become S, O/C becomes O, W/C becomes W, P/C becomes P, and stirring time becomes T, this change is made for the better expression of the mathematical model, and the cleaning of the graphics.

3.3 Preparation of shear-sensitive fluid

The formulations were prepared according to the steps presented in Figure 3.2, where the velocity of 11000 RPM corresponds to the low level of the Hamilton Beach mixer to simulate the fluid passing through the nozzles of the bit. The volume of 35 ml was selected as the volume enough to develop the rheological tests. The methodology to mix and create the material is the same as presented on the patent of Mintz and Irani (1983).

Figure 3.2 shows the process of preparation of the shear-sensitive fluids (SSF). First, two beakers with the non-aqueous and aqueous phase are presented (a); then, both contents are mixed (b) and took to the mixer (see the high shear apparatus and the container used to mix (c); (d) down at left is the mixture after 150 s of mixing. Figure 3.2e shows a formulation sample where a brine of 240000 ppm of NaCl was used to prove the behavior of

the SSF under high salt concentrations. That figure allows observing the resultant instability and precipitation of the clay under high salt concentration. That was caused by the cation exchange between the bentonite and the salt. The salt inhibits the swelling of the clay, as presented in Appendix A. Figure 3.2f present the original formulation without salt after applied high shear stress. The last figure (g) corresponds to the geometry used in the rheometer to run the rheological analyses.

.a. Clay+Olefin+Surfactant and HPAM+Water

b. Mixture before shear

c. Mixer

d. After high shear mix

e. Formulation +NaCl

f. Original Formulation

g. Plate-plate geometry
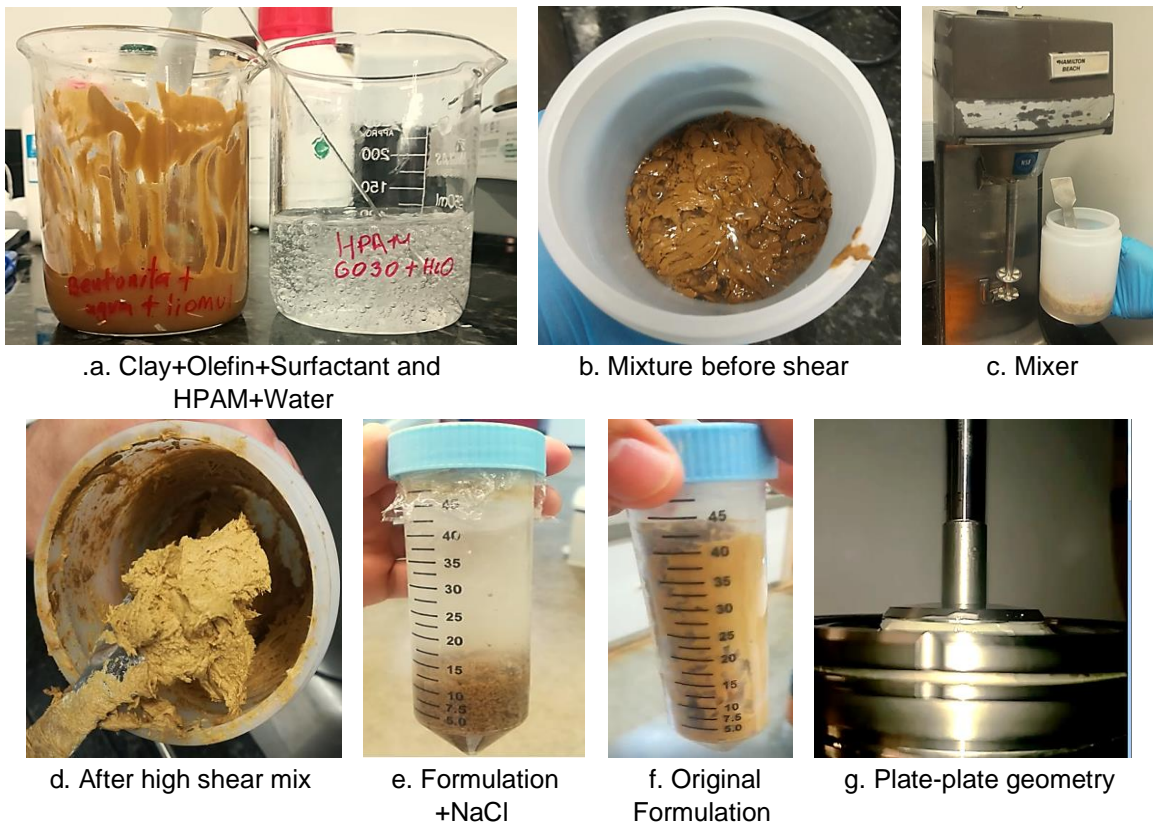
Figure 3.2 Process of preparation of the SSF

3.4   Rheological tests

Oscillatory shear tests were made for each sample at a constant temperature of 25 °C (to understand the behavior of the material). The use of the plate-plate geometry (P-35-Ti-L) is essential to avoid the slip effect and obtain more reliable data. The methodology presented in Appendix B was used to determine the optimum gap. The steps for the rheology tests are list in Figure 3.3.
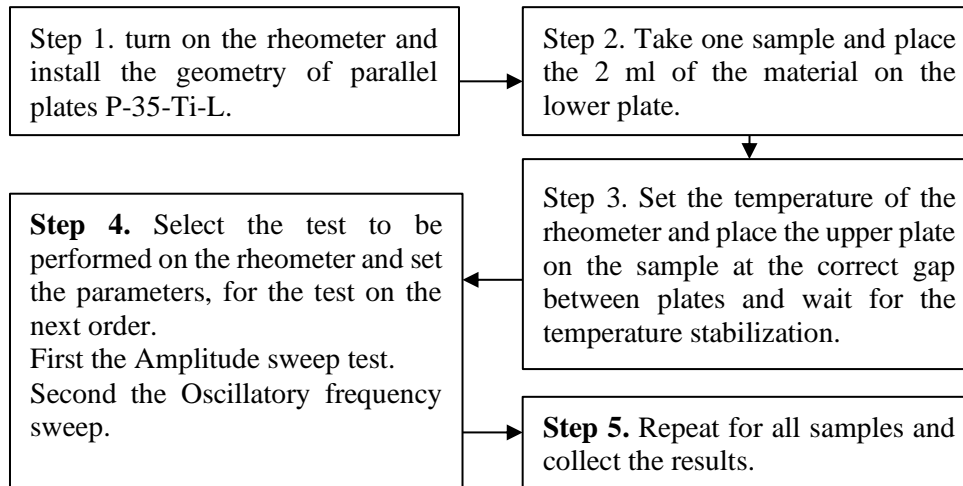
Step 1. turn on the rheometer and install the geometry of parallel plates P-35-Ti-L.	Step 2. Take one sample and place the 2 ml of the material on the lower plate.

Step 4. Select the test to be performed on the rheometer and set the parameters, for the test on the next order. First the Amplitude sweep test. Second the Oscillatory frequency sweep.	Step 3. Set the temperature of the rheometer and place the upper plate on the sample at the correct gap between plates and wait for the temperature stabilization.
	Step 5. Repeat for all samples and collect the results.

Figure 3.3 Flow diagram of laboratory rheology test

Once all the experiments were done, the next step is to develop the statistical analyses, focusing on the yield stress.

3.5   Statistical analyses from measured data

First, the equality of the average values of the yield stress of the samples with a significance level of 5% ($\alpha = 0.05$) is assumed for the statistical analyses. At this stage, the defined factors do not have a significant effect on the average response. This hypothesis is defined as follows.

$$H_0:\ \sigma_O = \sigma_P = \sigma_W\ = \sigma_T = 0$$

$$H_A:\ \sigma_O \neq \sigma_P \neq \sigma_W\ \neq \sigma_T \neq 0$$

The H_0 assumes that all factors (S/C, O/C, W/C, P/C, and T) have a null effect on the response (formulation yield stress), and the H_A considers that at least one factor has a significant effect on the response, the σ_i represent the mean response for each factor.

Following, ANOVA is made for the factorial statistical analysis, and the factors and their interactions on the response (yield stress) are studied. The elements presenting a significative effect on the response can be identified for a p-value of 0.05.

For the full factorial design, it is assumed that the yield stress (τ_y) response can be described by the model given by equation (3.1).

$$\tau_y = b_0 + b_1 * O + b_2 * W + b_3 * P + b_4 * T + b_{12} * O$$
$$* W + b_{13} * O * P + b_{14} * O * T + b_{23} * W$$
$$* P + b_{24} * W * T + b_{34} * P * T + \varepsilon$$

(3.1)

Where τ_y is the yield stress, b_i are the coefficients, ε is the random error (MONTGOMERY, 2004), the $O, W, P \ and \ T$ are the factors O/C, W/C, P/C, and T, respectively.

The model of equation (3.1) can be represented in a matrix by equation (3.2), as described by Teófilo and Ferreira (2006).

$$\hat{y} = X \ b$$

(3.2)

Where $\hat{y}$ is the vector of the responses (measured yield stress), b is the regression vector of the coefficients of the model, and X represents the matrix of the codified factors. One way to determine the values of b is by using the least-squares method defined by equation (3.3):

$$b = (X^t X)^{-1} X^t y$$

(3.3)

Where $(X^t X)^{-1}$ is the inverse matrix of the product of the transposed matrix X with herself.

The value of the effects corresponds to the double of the value of each coefficient of the model, except for b_0, whose value is the same for its effect. The effects errors for experiments without repetitions are calculated by identifying the non-significative interactions using the equation (3.4):

$$V(ef) = \frac{\sum_{i=1}^{l} e_{fi}^2}{l}$$

(3.4)

Where e_{fi} are the experimental effects errors, and l corresponds to the total number of effects considered.

The identification of the factors that has a low effect on the response is made using the Pareto plot. For non-replicated experiments, it is useful the combination of the Pareto plot with the margin of error, showed as a straight orange line on the Figure 3.4a determined by the Lenth method (LENTH, 1989), that is determined by the equation (3.5) to equation (3.7).

$$s_o = 1.5 * median|C_j|$$

(3.5)

$$PSE = 1.5 * median|C_j|, where \ |C_j| < 2.5 s_o$$

(3.6)

$$ME = t_{1-\alpha,d} * PSE \tag{3.7}$$

where C_j denote the corresponding effects, s_o is a value determined to calculate the PSE, the PSE is the pseudo standard error of the contrasts, $t_{1-\alpha,d}$ is the quantile of a t distribution and d denote the degree freedom where $d = m/3$, and the ME is the margin of error.

A routine in MATLAB was designed to facilitate all the calculus of all terms discussed here, and it is presented in Appendix D.

Graphic techniques are used to prove if the statistical assumptions are fulfilled. First, the assumption of normality was checked by plotting the residuals in a normal probability paper. If the points are normally distributed on a straight line that passes through quartile 1 and quartile 3, the values satisfy the assumption (Figure 3.4b). The independence assumption was checked by plotting the residuals from the model with the predicted values. If the behavior of the points is random within a horizontal band, this indicates that the assumption is fulfilled, see Figure 3.4c.

a.   **Pareto plot representation of the effects. Adapted from Montgomery (2004)**

b.   **Normal Plot of residuals**

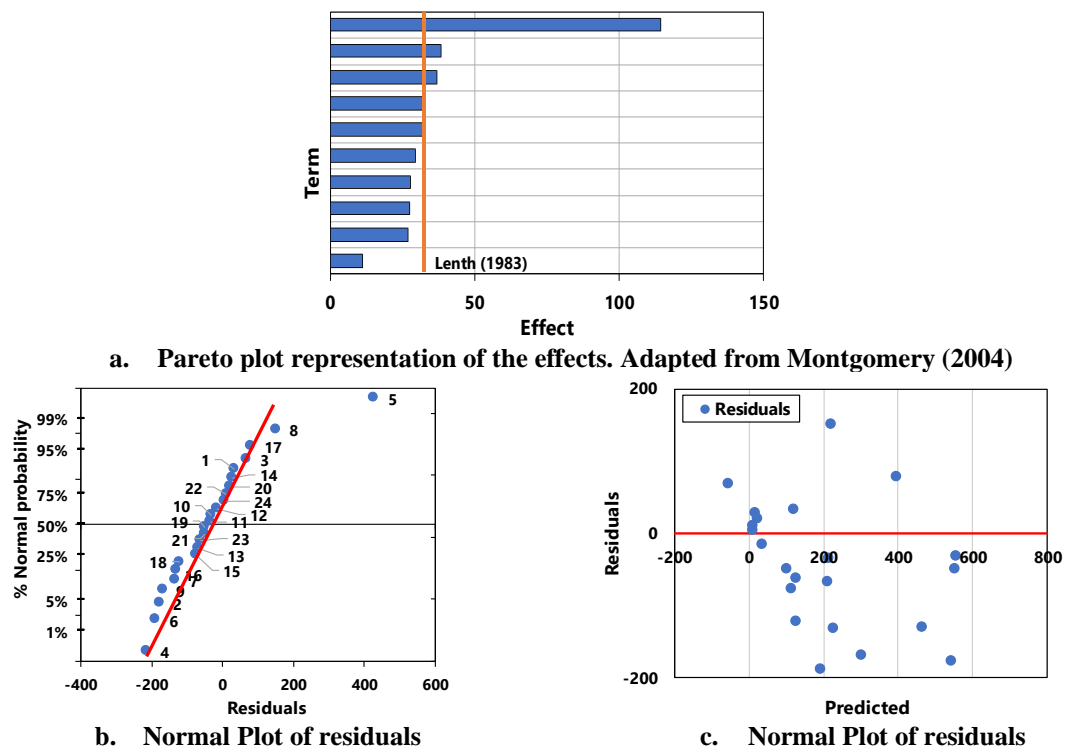c.   **Normal Plot of residuals**

Figure 3.4 Pareto plot representation of the effects. Adapted from Montgomery (2004)

A non-visual test called the Grubbs test defines the standardized residuals and is used to identify the outlier points (Equation (3.8). This test admits a normal distribution and compares the distance measured in standard deviations. If this value is greater than 3 or 4 units,

the point is considered an outlier. After identifying these points, it can be defined if there are errors in the execution of the experiment.

$$Grubbs = \frac{|y_i - \bar{y}|}{\sqrt{MS_E}}$$

(3.8)

Finally, a plot of predicted values versus measured values is made to visually identify the fitting model (Figure 3.5).
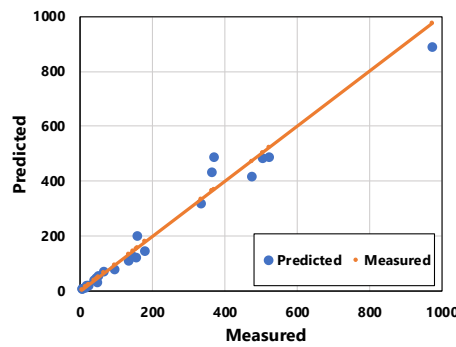
Figure 3.5 Predicted versus measured values

A graph of main effects and interactions is made to optimize the formulation. The first one shows the level for the components, and the second graph turns possible to analyze the combination of two or more factors, and the optimal concentration recommended to achieve a high value of the response.

The main factor effect is represented graphically, as in Figure 3.6, with the horizontal axis containing the factor levels and the vertical axis containing the mean of the response obtained at the corresponding levels. For a high interaction, the lines have a very different slope, and if there is no interaction, the lines have similar slopes and are approximately parallel (MONTGOMERY, 2004).

Figure 3.6 Mean of response versus level of the factors

4 RESULTS AND DISCUSSIONS

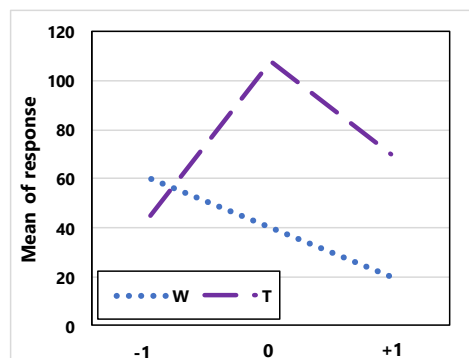In this chapter, the rheological data (see Chapter 2 -Item 2.5) from the tests carried out in the laboratory are presented, and the statistical studies are designed to determine what components of the formulation can optimize the yield stress.
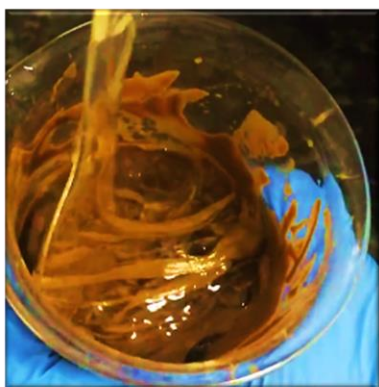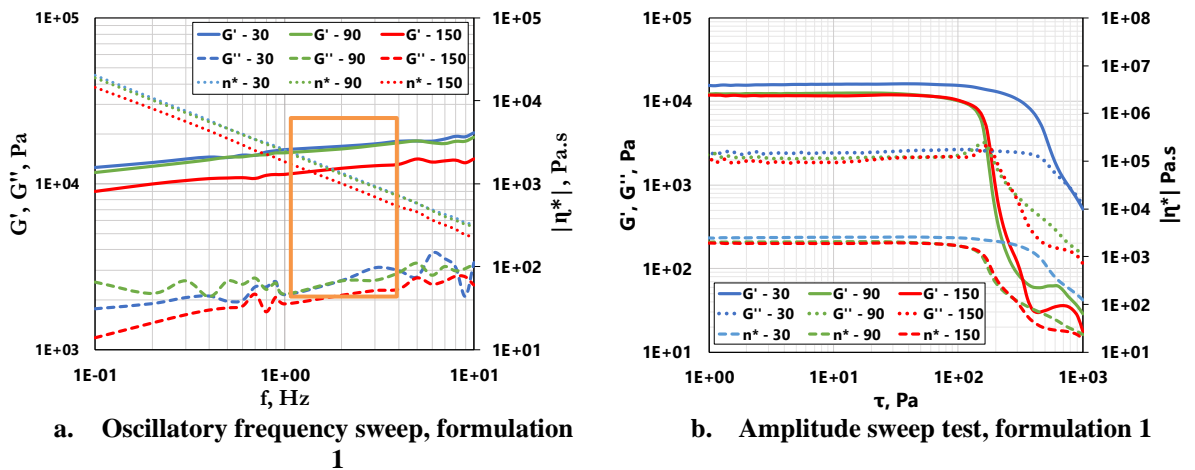
4.1.1 Oscillatory shear tests

Oscillatory shear tests were run to identify the useful range of stress and frequency to extract the data to determine the yield stress.

Oscillatory tests were performed for all samples, using a sensor gap between plates of 0.8 mm (see Appendix B) and 25 °C. This temperature was chosen to evaluate the material at laboratory conditions and understand its behavior.
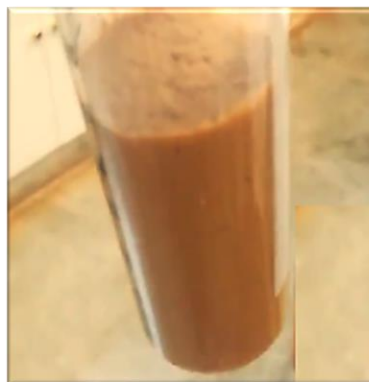
Figure 4.1 presents the results for Formulation 1 (see Table 3.2). Figure 4.1a shows an oscillatory frequency sweep (OFS) test, where the frequency varies from 0.1 to 10 Hz, and the G' (elastic modulus), G'' (viscous modulus), and $|\eta^*|$ (Complex viscosity) are recorded. The results indicate a linear increase of G' and G'' while frequency increases. Below frequencies of 1 Hz, G'' decreased almost linearly, and for values higher than 1 Hz, G'' started to increase. The use of a frequency between 1 and 4 Hz corresponds to a linear behavior for both G' and G'' (highlighted by the orange rectangle). Therefore, 1 Hz was selected for the amplitude sweep test.

Figure 4.1b shows an amplitude sweep test for Formulation 1. The shear stress is varied from 1 Pa to 1000 Pa, with a frequency of 1 Hz to evaluate both G', G'' and $|\eta^*|$. In this case, sample 2 and sample 3 present similar values for G', G'', and $|\eta^*|$, indicating no difference in stir the material for 90 s or 150 s. Sample 1, in this test, shows the best behavior and higher stability to high shear stress.

Figure 4.1c shows sample 1 (mixed for 30 s), sample 2 (mixed for 90 s), and sample 3 (mixed for 150s) as items c, d, and e, of Figure 4.1 respectively. Although all samples have the same composition, sample 1 is physically different from samples 2 and 3. Sample 1 was not homogenously mixed, and both portions looked almost like liquid, while sample 2 show a viscous appearance, and sample 3 seemed like a paste.

a. Oscillatory frequency sweep, formulation 1

b. Amplitude sweep test, formulation 1

c. Sample 1, 30 s of stir

d. Sample 1, 90 s of stir

e. Sample 1, 150 s of stir

Figure 4.1 Result of oscillatory shear tests

The test behavior for all samples is very similar to that presented for Formulation 1 (samples 1, 2, and 3) (see Figure 4.2). The frequency of 1 Hz was selected to run the amplitude sweep test for all other samples, and the results showed that the value of G' is 4 to 11 times higher than G'' for all samples and presents a solid-like behavior until their respective yield stress was overcome. The stress of 1000 Pa is enough to evaluate the highest yield stress related to the tested samples.

a. Oscillatory frequency sweep, formulation 2

b. Amplitude sweep test, formulation 2

Figure 4.2 Results of Oscillatory tests for all samples (Continues)

c. **Oscillatory frequency sweep, formulation 3**

d. **Amplitude sweep test, formulation 3**
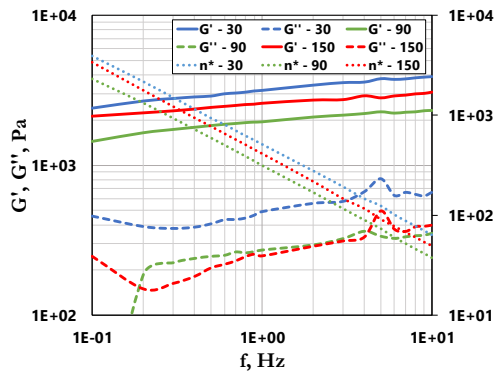
e. **Oscillatory frequency sweep, formulation 4**
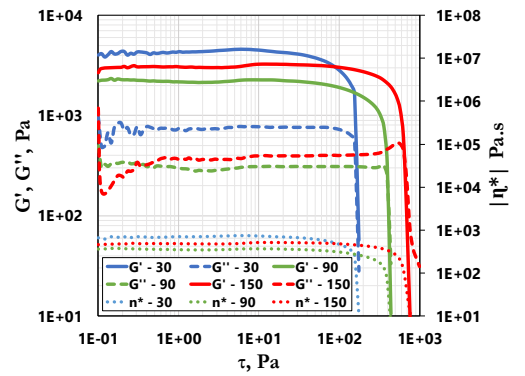
f. **Amplitude sweep test, formulation 4**
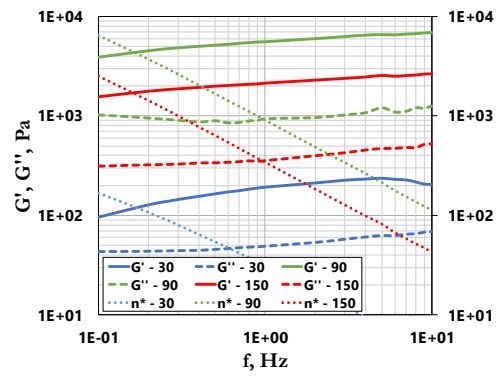
g. **Oscillatory frequency sweep, formulation 5**
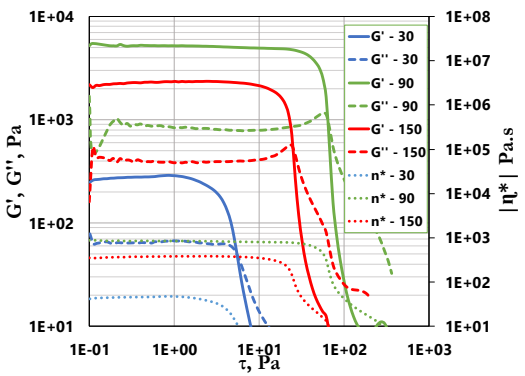
h. **Amplitude sweep test, formulation 5**
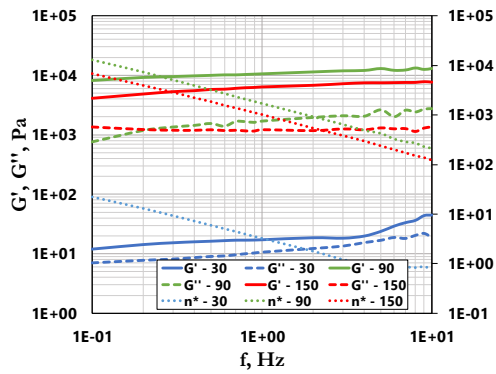
i. **Oscillatory frequency sweep, formulation 6**
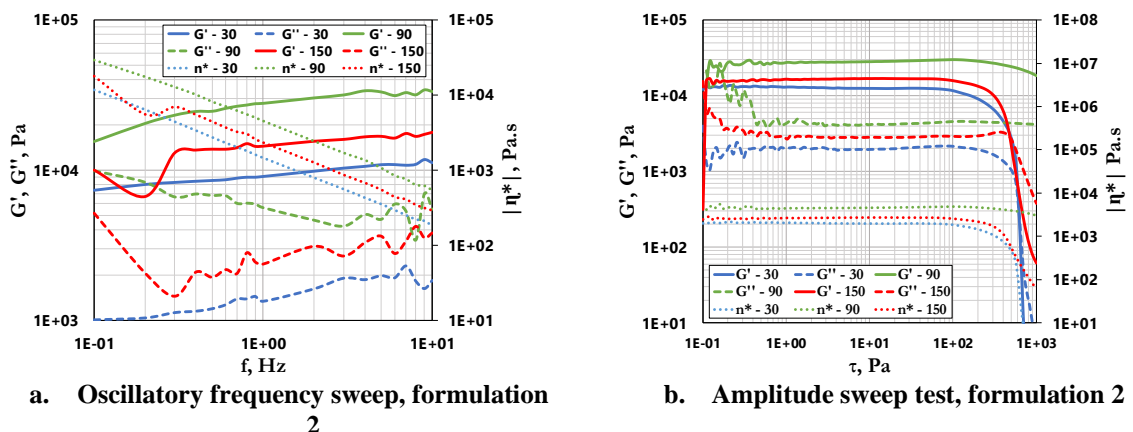
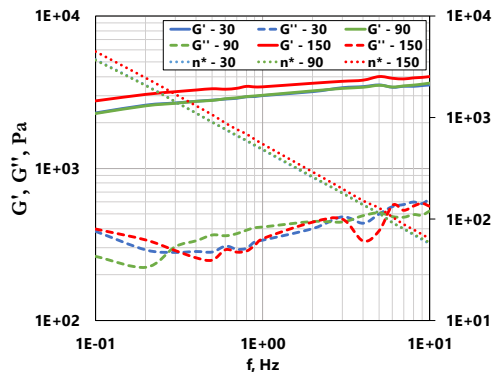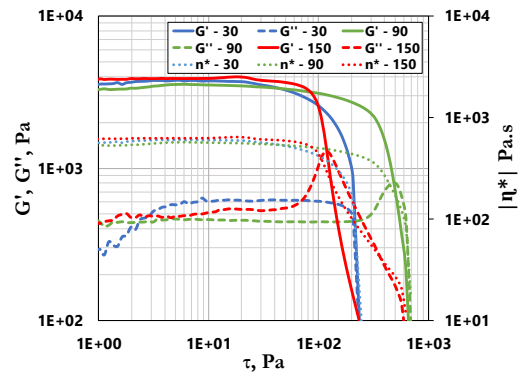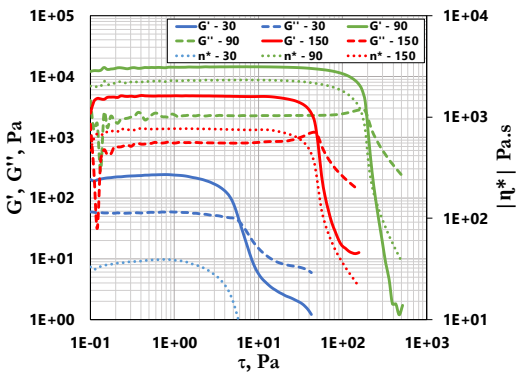j. **Amplitude sweep test, formulation 6**

Figure 4.2 Results of Oscillatory tests for all samples (Continues)

k. Oscillatory frequency sweep, formulation 7

l. Amplitude sweep test, formulation 7

m. Oscillatory frequency sweep, formulation 8

n. Amplitude sweep test, formulation 8
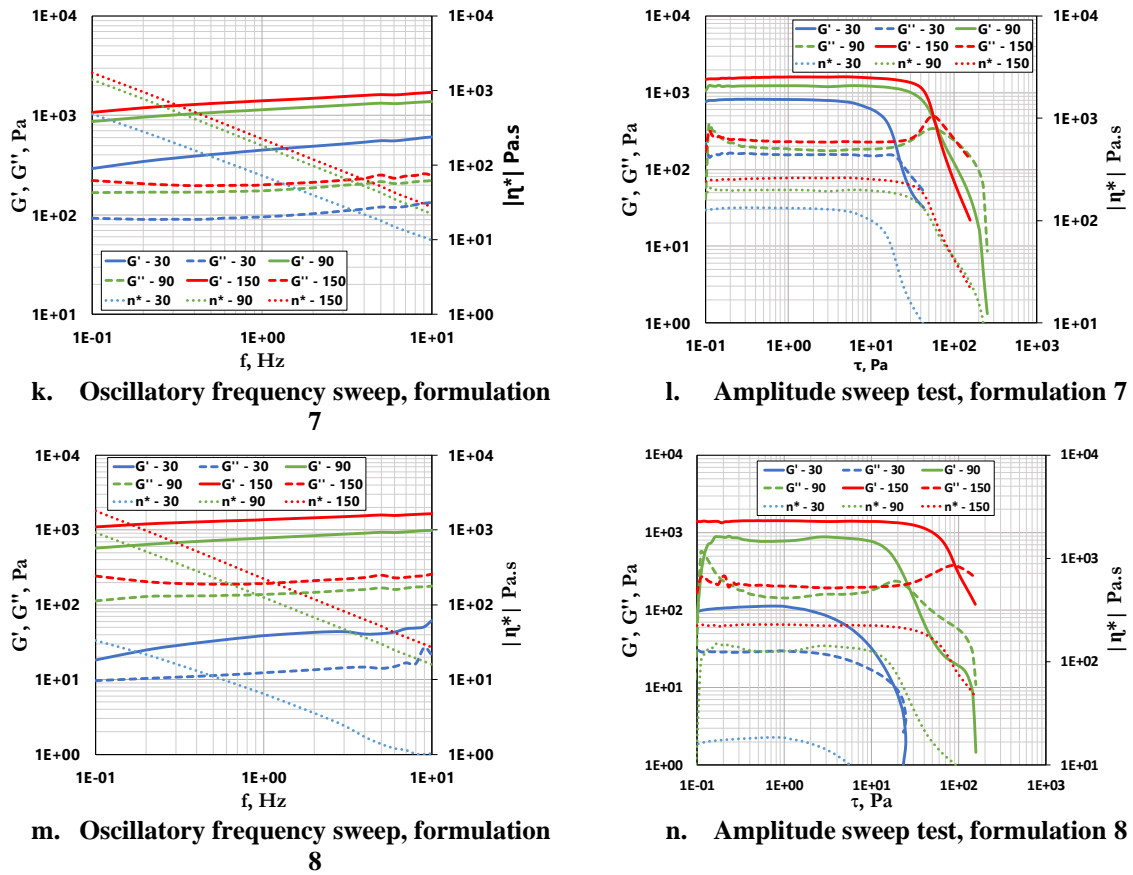
Figure 4.2 Results of Oscillatory tests for all samples

4.1.2 General graphic results for yield stress

Once the data was collected from the rheological studies, the yield stress was found by two methods described in Chapter 2.5, the elastic method and the DIN 51810-2 standard. The graphic results are shown below. Figure 4.3 shows the elastic method results, and Figure 4.4 shows the results of the DIN 51810-2 norm. Figure 4.5 summarizes all results.

One can see from Figure 4.3 that the best results were found for samples where the values reached more than 500 Pa. It can be seen for sample 5 (975 Pa), sample 4 (503 Pa), and sample 12 (523 Pa), which were almost two times higher when compared to other samples. One common results of samples 4 and 5 is that they have a low level of O/C and a high level of P/C and stirring times between 30 and 90 seconds. For samples 13 and 16 that present the lower values of yield stress, it is shared a high level of O/C, a low level of W/C, and a T of 30 s.
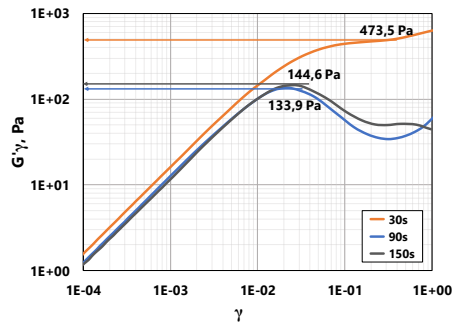
a. **Formulation 1 - Samples 1, 2 and 3**
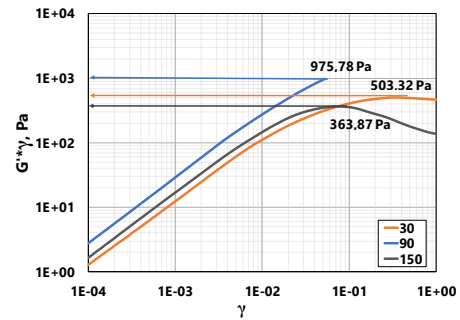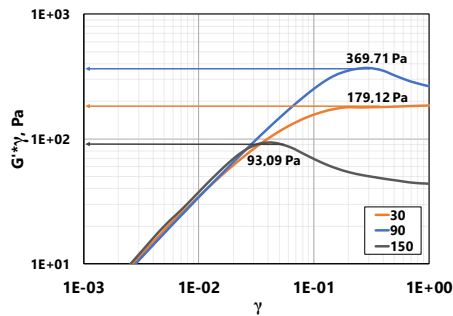
b. **Formulation 2 - Samples 4, 5 and 6**

c. **Formulation 3 - Samples 7, 8 and 9**
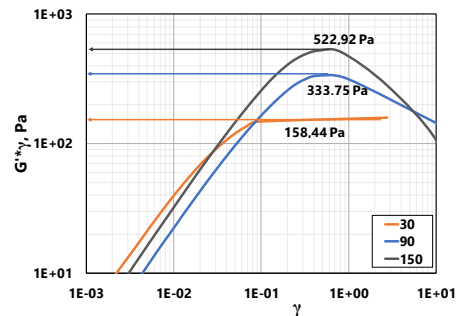
d. **Formulation 4 - Samples 10, 11 and 12**
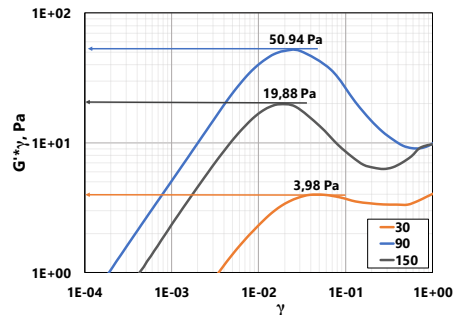
e. **Formulation 5 - Samples 13, 14 and 15**
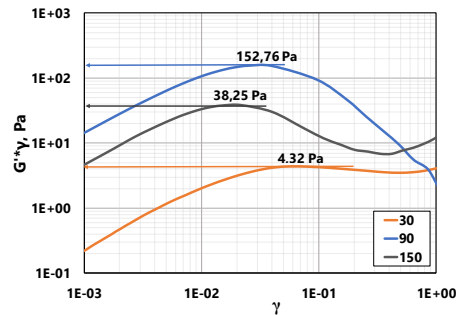
f. **Formulation 6 - Samples 16, 17 and 18**
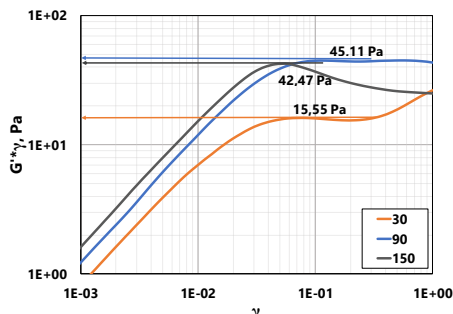
g. **Formulation 7 - Samples 19, 20 and 21**
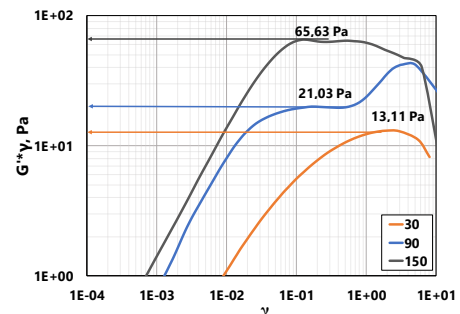
h. **Formulation 8 - Samples 22, 23 and 24**

Figure 4.3 Results of the elastic method

The results from Figure 4.4 allow concluded that the samples with the highest yield stress are sample 5 (435.34 Pa), sample 6 (131.12 Pa), and sample 1 (150.97 Pa). These samples have in common that the O/C level is low, the water level is high, as is the P/C level. The samples that present the lowest yield stress value are 13 (1.94 Pa), 16 (1.73 Pa), and 22 (1.79

Pa), and the common factor is a high level of O/C and a stirring time of 30 seconds. These graphs show again that the level of olefin in the formulation has a significant effect and that the higher is the O/C quantity, the lower is the reached yield point. These observations are verified with statistical analysis.

a. Formulation 1 - Samples 1, 2 and 3

b. Formulation 2 - Samples 4, 5 and 6

c. Formulation 3 - Samples 7, 8 and 9

d. Formulation 4 - Samples 10, 11 and 12

e. Formulation 5 - Samples 13, 14 and 15

f. Formulation 6 - Samples 16, 17 and 18

g. Formulation 7 - Samples 19, 20 and 21

h. Formulation 8 - Samples 22, 23 and 24
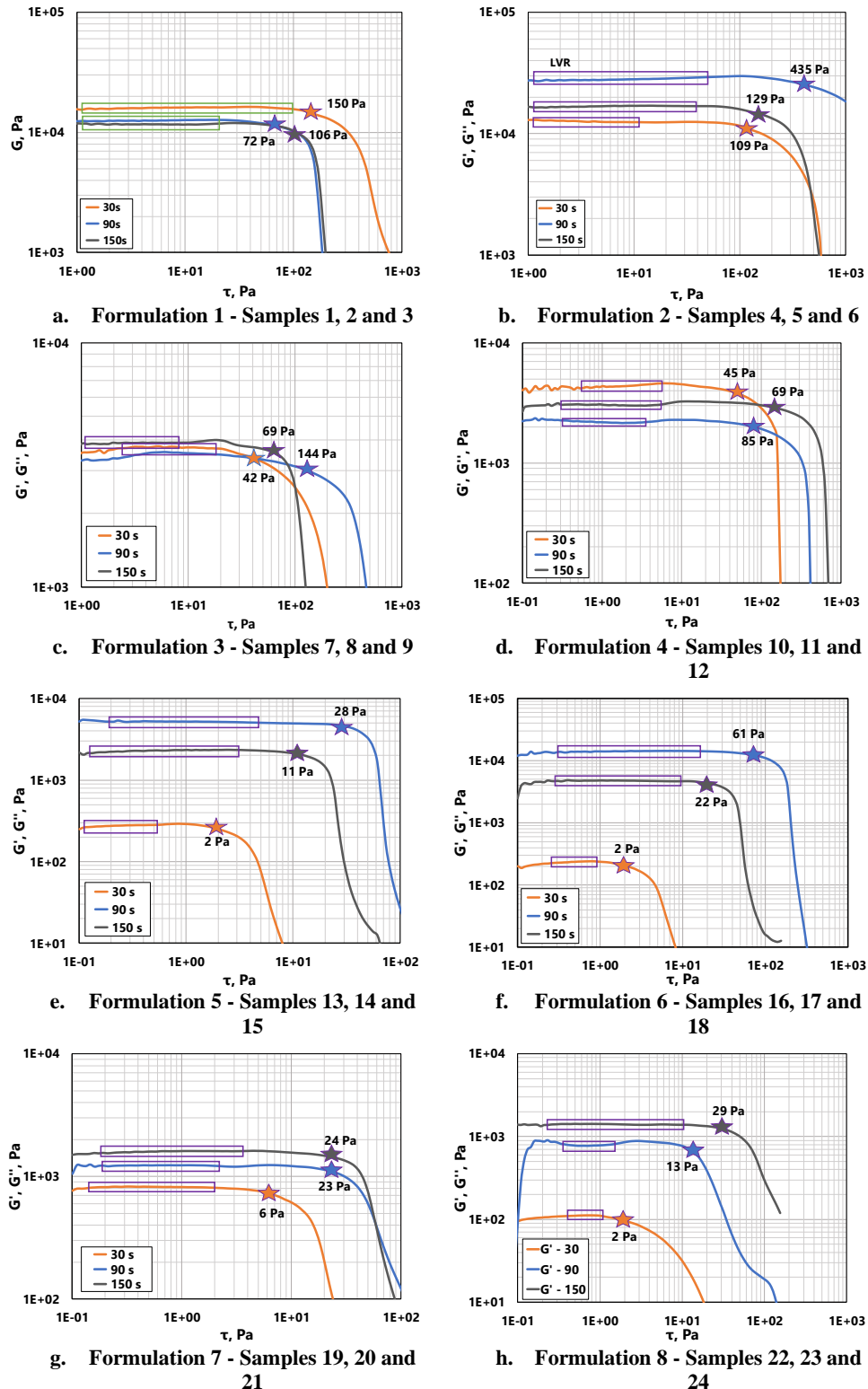
Figure 4.4 Results of the DIN 51810-2 norm

Figure 4.5 shows the results of both methods, Din 51810-2 and the elastic stress, where it is in accordance that the high value for yield stress was achieved by sample 5. Some features observed for data obtained by the DIN method are the following: the high yield stress for sample 1 at 30 s, for samples 5, 8, 14, and 17 at 90 s, and for samples 12 and 24 at 150 s. Among Elastic method results, it can be highlighted that the higher values for 30 s of stir were achieved by sample 1, for 90 s by sample 2, 8, 14, 17, and 20, and for 150 s by samples 12 and 24. Both methods showed the same behavior, indicating consistency, although the calculated values were not exactly the same. The results can be evaluated visually on the bar graph of where both methods are plotted, and the differences are easily detected, where the best results are those above 100 Pa.
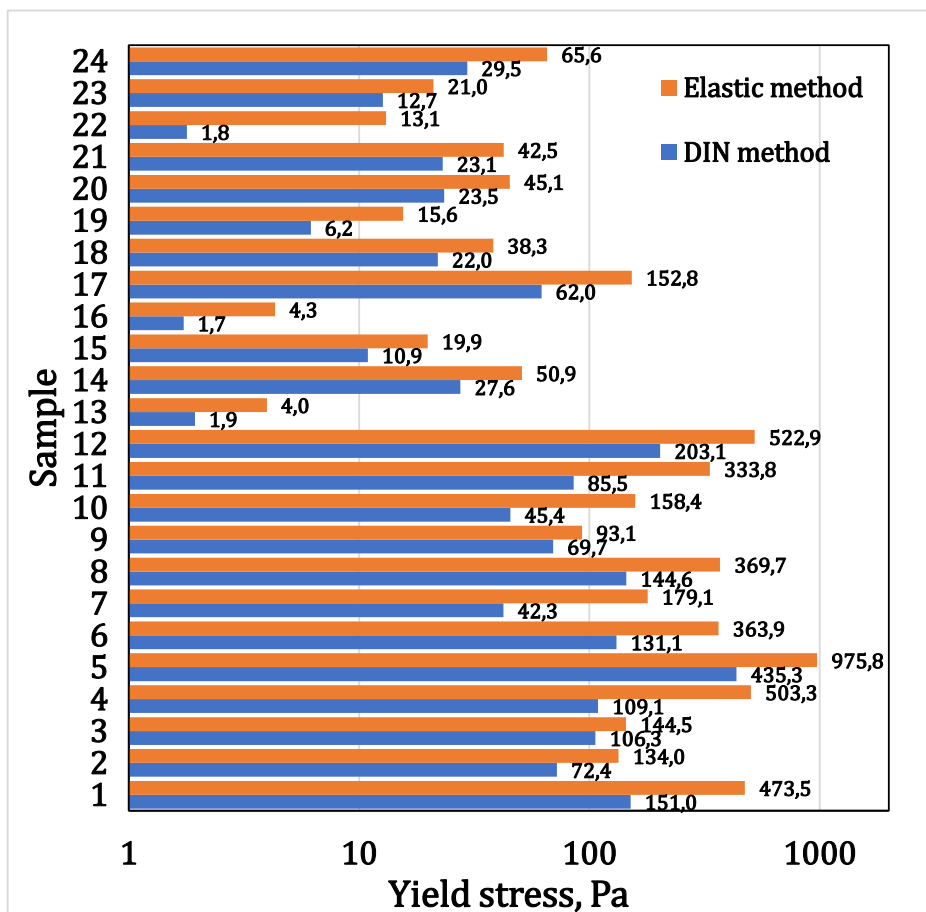
Figure 4.5 Bar graph of yield stress for DIN and Elastic method

4.1.3   Statistical analyses and model construction from complete data

The elastic method was designed for viscoelastic materials with high viscosity, then the results of this method are used to perform the statistical analyses. First, the analysis of variance ANOVA, recommended in Chapter 2-Item 2.6, is made to identify which factors or interactions have statistically significant differences in the response variable. Then the

coefficients of the model, the effects, and the residuals are calculated. With these data, a study is carried out following Chapter 3 – Item 3.6. Subsequently, the model can be optimized, eliminating the factors that do not significantly influence the response, and finally, the optimal composition is defined to achieve the highest yield stress.

Table 4.1 shows the ANOVA for all factors and interactions. The values with a confidence level lower than 0.05 show a significant effect on the response. The coefficients of determination are indicators of how well the factors can explain the response of the experiment. R^2 was 100%, showing a perfect match among the factors and the yield stress. When using all factors and interaction, it could indicate a potential overfitting problem. However, Pred R^2 was 0%, which indicates that the model determined with all factors and interactions is overfitting, requiring some factors exclusion. That exclusion justifies the low possibility of thoroughly explaining the interaction between three or four factors at three or four levels, and then these interactions are the first to be excluded.

Table 4.1 ANOVA for principal factors and all interactions

Source	Sum. Square	DF	Mean square	Fc	p-value
O	595029	1	595029	-	-
W	42098	1	42098	-	-
P	104192	1	104192	-	-
T	48632	2	24316	-	-
O*W	31587	1	31587	-	-
O*P	75602	1	75602	-	-
O*T	21465	2	10732	-	-
W*P	29520	1	29520	-	-
W*T	45862	2	22931	-	-
P*T	53044	2	26522	-	-
O*W*P	14695	1	14695	-	-
O*W*T	32244	2	16122	-	-
O*P*T	36838	2	18419	-	-
W*P*T	102540	2	51270	-	-
O*W*P*T	61535	2	30768	-	-
Model	1294884	23	56299,3	R^2	100,00%
Error	0	0	-	Adj R^2	-
Total	1294884	23	56299,3	Pred R^2	0,00%

Table 4.2 shows the ANOVA for all factors and two levels of interaction. In this case, the value that fulfills the condition of the p-value is the olefin, and the values that have a low p-value are P, the interaction O*P, the factor W, O*W, W*P, and finally P*T respectively. The R^2 is 80.86%, the Adj R^2 is 51.08%, and finally, the Pred R^2 is 0%. These values indicate that although the first correlation coefficient is high, the second (Adj R^2) coefficient indicates

that possibly there is an over-adjustment of the factors, which is confirmed by the third coefficient (Pred R^2). These results indicate that the found model does not present reliability, and then other factors or interactions need to be excluded.

Table 4.2 ANOVA for principal factors and second level of interactions

Source	Sum. Square	DF	Mean square	Fc	p-value
O	595029	1	595029	21,607	0,0012
W	42098	1	42098	1,529	0,2476
P	104192	1	104192	3,783	0,0836
T	48632	2	24316	0,883	0,4465
O*W	31587	1	31587	1,147	0,3121
O*P	75602	1	75602	2,745	0,1319
O*T	21465	2	10732	0,390	0,6881
W*P	29520	1	29520	1,072	0,3275
W*T	45862	2	22931	0,833	0,4658
P*T	53044	2	26522	0,963	0,4178
Model	1047032	14	74788,0	R^2	80,86%
Error	247853	9	27539,2	Adj R^2	51,08%
Total	1294884	23	56299,3	Pred R^2	0,00%

The process for checking if the computed model meets the statistical assumptions is following described in Figure 4.6. The procedure serves to identify possible outliers, factors without significant effects on the response, and the representativeness of the measured data by the computed model (see Figure 4.6).

Figure 4.6a shows that the normality of the residuals is fulfilled since most points are distributed in the central part of the graph. Besides, there are no outliers. Point 5 could be classified as an outlier value, but this value cannot be ignored since it corresponds to the highest yield stress among experimental data. Through Figure 4.6b, one can verify that the residuals do not show any obvious pattern of distribution concerning the predicted values, so the principle of variability is fulfilled. Summarizing, we can be confident that the data collected during the experiment are reliable to continue with the model optimization process.

The continuity of the model optimization demands to find the values that do not have significant effects on the response and remove them from the model; for this, the normal distribution of factors is determined, and the result is shown in Figure 4.6c. In this case, one can see that the values that could have a significant effect are O, O*T, W*T, and T. Figure 4.6 shows the Pareto plot that is used to confirm this assumption. It shows a bar graph with absolute values of the effects, where a red line identifies the margin of error from which an effect is considered significant. In this case, the only one that exceeds the margin of error is the olefin.

The lowest value is the stirring time, which was entirely unexpected since it was believed that stirring time would have a more significant influence on the final response. Other values to be considered for the model optimization were P, O*P, W*T, P*T, and W.

Figure 4.6e shows a plot of predicted values versus measured values, where the red line represents the real values measured in the laboratory, and the blue points correspond to the values calculated by the model presented in Table 4.3. A cluster of points can be seen that at the beginning, most of the values are below 100 Pa, compared to large values as 900 Pa justifying the presented behavior.

a.   Normal Plot of residuals

b.   Residuals versus predicted values

c.   Normal plot of effects

d.   Pareto plot
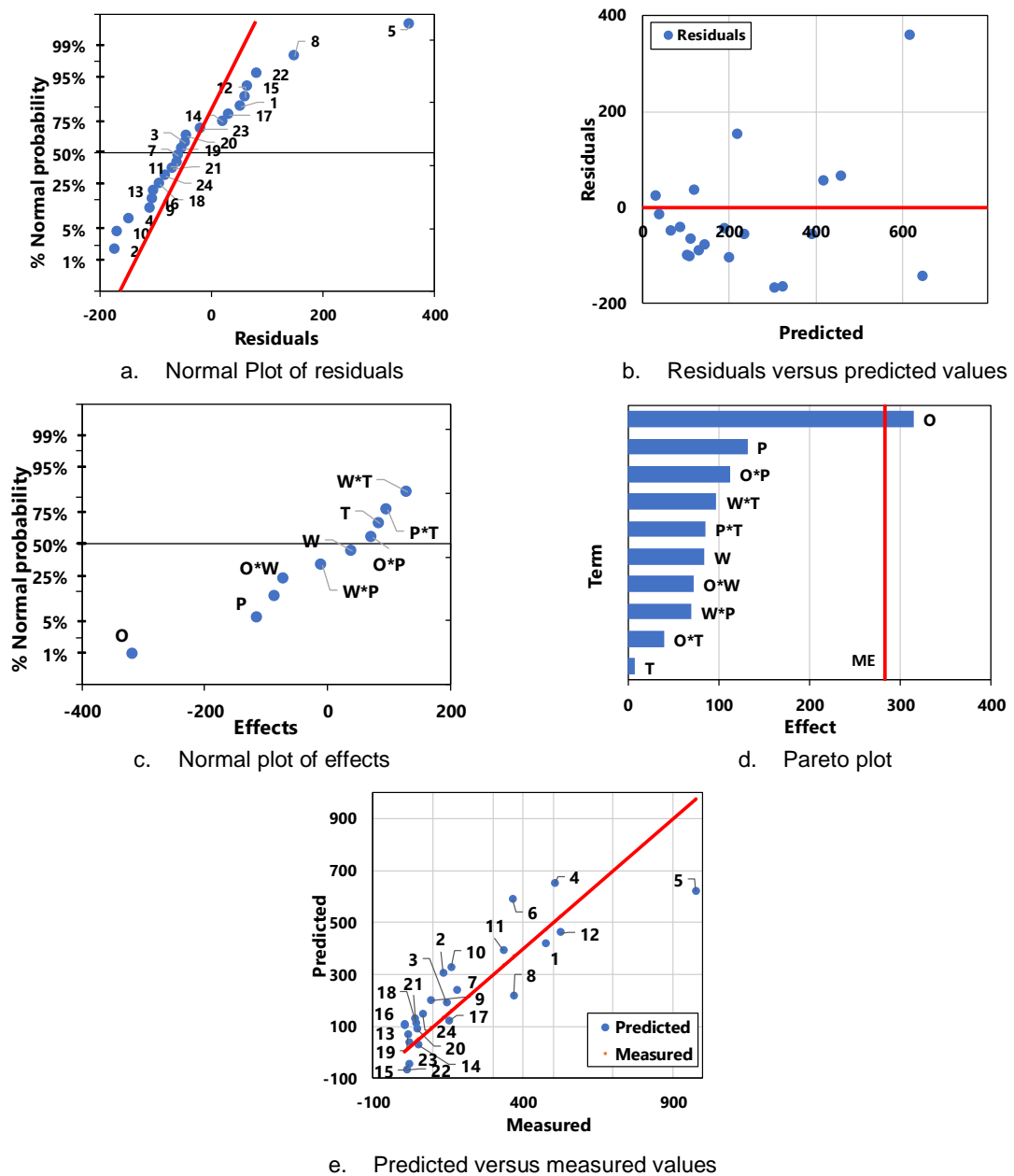
e.   Predicted versus measured values

Figure 4.6 Significance of the effects, residuals, and model fitting for all factors and second interactions

Table 4.3 shows the residuals and the standardized residuals (equation (3.8)). From the standardized residuals, we can identify if exists outliers. As none of the calculated values exceeds 3 units, there are no outliers from the laboratory tests. The model's codified coefficients and the calculated effects are shown, and the model generated from these coefficients is presented in the lower right part of the table. The error was determined by equation (3.4). As seen previously in the ANOVA, this model does not reliably represent the responses obtained in the laboratory and therefore needs to be optimized.

Table 4.3 Model with all factors and second interactions

Sample	Measured Value	Predicted Value	Residual	Standardized residuals	Interaction	Codified Coefficients	Effects
1	473.51	420.57	52.94	0.32		196.88	
2	133.98	305.55	-171.57	-1.03	O	-157.46	-314.92
3	144.49	190.54	-46.04	-0.28	W	-41.88	-83.76
4	503.32	649.28	-145.96	-0.88	P	65.89	131.78
5	975.78	619.73	356.06	2.15	T	-3.80	-7.59
6	363.87	590.17	-226.30	-1.36	O*W	36.28	72.56
7	179.12	237.33	-58.21	-0.35	O*P	-56.13	-112.25
8	369.71	219.38	150.33	0.91	O*T	19.96	39.91
9	93.09	201.42	-108.33	-0.65	W*P	-35.07	-70.14
10	158.44	325.75	-167.30	-1.01	W*T	48.53	97.07
11	333.75	393.26	-59.51	-0.36	P*T	42.73	85.47
12	522.92	460.78	62.14	0.37	error	30.15	
13	3.98	105.44	-101.46	-0.61	Model: $y_{calc} = 196.88 - 157.46*O -$		
14	50.94	30.33	20.61	0.12	$41.88*W + 65.89*P - 3.8*T +$		
15	19.88	-44.77	64.65	0.39	$36.28*O*W - 56.13*O*P + 19.96*$		
16	4.32	109.64	-105.32	-0.63	$O*T - 35.07*W*P + 48.53*W*T +$		
17	152.76	120.00	32.76	0.20	$42.73*P*T + 30.15$		
18	38.25	130.36	-92.11	-0.56			
19	15.55	67.31	-51.76	-0.31			
20	45.11	89.27	-44.15	-0.27			
21	42.47	111.23	-68.76	-0.41			
22	13.10	-68.77	81.87	0.49			
23	21.03	38.65	-17.62	-0.11			
24	65.63	146.08	-80.45	-0.48			

4.1.4 Statistical Analyses and model construction from filtered data

Based on the previous analysis, factors and interactions were filtered, and statistical analyses were carried out again. Table 4.4 shows the analysis of variance for filtered factors and second level interactions. The correlation coefficients R^2, Adj R^2, Pred R^2 were 70.73%, 55.11%, and 42.68%, respectively. These values are better when compared with the ANOVA result for all factors, especially the Pred R^2, which shows that the model has a better level of fit.

Table 4.4 ANOVA with filtered data

Source	Sum. Square	DF	Mean square	Fc	p-value
O	595029	1	595029	23.5465	0.0001
W	42098	1	42098	1.6659	0.2096
P	104192	1	104192	4.1231	0.0540
O*P	75602	1	75602	2.9917	0.0971
W*T	45862	2	22931	0.9074	0.4175
P*T	53044	2	26522	1.0495	0.3663
Model	915828	8	114479	R^2	70.73%
Error	379056	15	25270	Adj R^2	55.11%
Total	1294884	23	56299	Pred R^2	42.68%

Table 4.5 shows the residuals and the standardized residuals. The latter allowed to identify that none of the calculated values exceeds 3 units, and no outliers were found from these new filtered values. The model's codified coefficients, the calculated effects, and the model generated from these coefficients are presented in the table.

Table 4.5 Optimized Model with Filtered Data

Order	Measured Value	Predicted Value	Residual	Standardized residuals	Interaction	Codified Coefficients	Effects
1	473.51	394.34	79.18	0.50		196.88	
2	133.98	303.07	-169.09	-1.06	O	-157.46	-314.92
3	144.49	211.81	-67.32	-0.42	W	-41.88	-83.76
4	503.32	552.91	-49.59	-0.31	P	65.89	131.78
5	975.78	547.10	428.68	2.70	O*P	-56.13	-112.25
6	363.87	541.30	-177.43	-1.12	W*T	48.53	97.07
7	179.12	213.51	-34.39	-0.22	P*T	42.73	-89.66
8	369.71	219.31	150.40	0.95	error	28.87	
9	93.09	225.11	-132.02	-0.83		Model:	
10	158.44	372.08	-213.63	-1.34			
11	333.75	463.34	-129.58	-0.82			
12	522.92	554.60	-31.69	-0.20			
13	3.98	191.67	-187.70	-1.18			
14	50.94	100.41	-49.47	-0.31			
15	19.88	9.15	10.73	0.07			
16	4.32	125.74	-121.42	-0.76			
17	152.76	119.94	32.83	0.21			
18	38.25	114.13	-75.88	-0.48			
19	15.55	10.84	4.71	0.03			
20	45.11	16.65	28.47	0.18			
21	42.47	22.45	20.02	0.13			
22	13.10	-55.09	68.19	0.43			
23	21.03	36.17	-15.14	-0.10			
24	65.63	127.44	-61.81	-0.39			

Model:
$$y_{calc} = 196.88 - 157.46 * O - 41.88 * W + 65.89 * P - 56.13 * O * P + 48.53 * W * T + 42.73 * P * T + 28.87$$

Figure 4.7a shows that the normality of the residues is fulfilled since most points are distributed in the central part of the graph, and there are no outliers. From Figure 4.7b, it

can be verified that the residuals do not show any obvious pattern of distribution concerning the predicted values, so the principle of variability is fulfilled. Figure 4.7c shows the values that can have a significant effect are O, and P, and from Figure 4.7d, one can see the only one that exceeds the margin of error is O, and P. Figure 4.7e shows the graph of predicted values versus calculated values.

a. Normal Plot of residuals

b. Residuals versus predicted values

c. Normal plot of effects
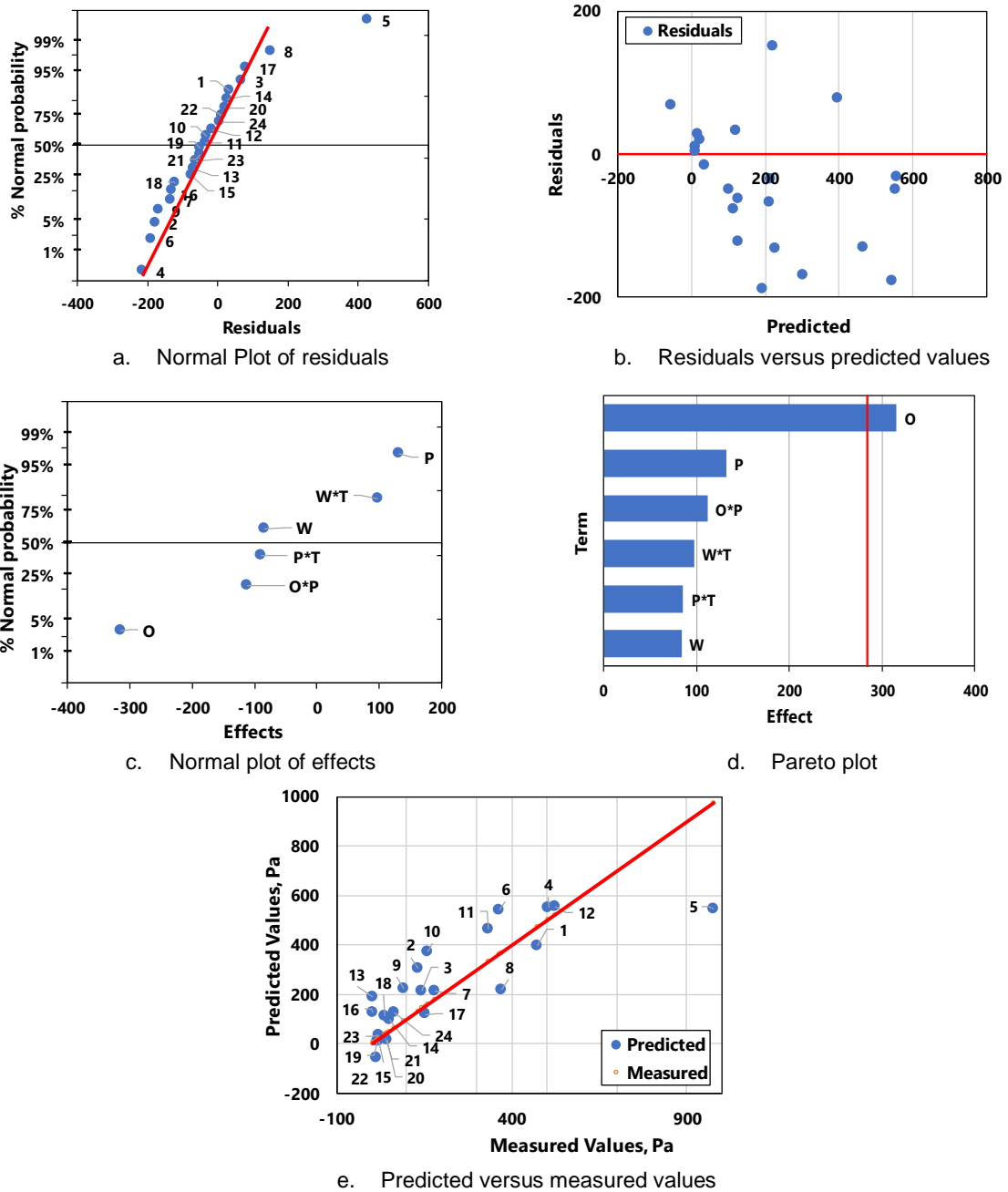
d. Pareto plot

e. Predicted versus measured values

Figure 4.7 Significance of the effects, residuals, and model fitting for filtered values

4.1.5 Optimization of the formulation

The process of optimization was based on the graphic of the mean response vs. levels. Figure 4.8 shows the effects of primary factors and second level of interactions; in Figure

4.8a, one can see that when Olefin increase from a low level (-1) to a high level (+1), the yield stress is reduced 86%; from an average of 350 Pa to a 50 Pa. The same occurred for water, for which the yield stress changed from 239 Pa to 155 Pa (35 % reduction). In the polymer case, a contrary effect was seen, and the yield stress increased 50% from 131 Pa to 263 Pa. There are two sections for the stirring time, the first one from the low to the medium level, which presents an increase of 65% (from 169 Pa to 260 Pa) and then, from the medium to the high level, which reduces 58%, from 260 Pa to 164 Pa. From this graph, one can conclude that the optimal conditions to reach the highest yield stress are adding a low level of olefin, a low level of water, a high level of polymer, and a medium level of stirring time.

Figure 4.8b shows the interaction between olefin and water. Since the slopes in the graphs do not cross and are similar, one can conclude that there is no interaction between them and that the best results for yield stress are achieved when there is a low level of olefin and a high level of water. Figure 4.8c shows the interaction between olefin and polymer, where it can be concluded that there is no interaction between these factors and that with the lowest level of olefin and the highest level of polymer, the highest yield stress is found. Figure 4.8d shows that there is no interaction between the polymer and water, and to obtain the best yield stress value, a high level of polymer and a low level of water is needed.

Figure 4.8e, f and g, show that there is a little interaction between the olefin, water, and polymer factors with the stirring time since, in some cases, the curves cross to each other. The one that presents a more significant interaction is the water with the stirring time since its high and low-level curves cross, and each of them has a different slope. Therefore, studying in more detail, it is possible to find a relationship between the stirring time and the highest yield stress reached by the formulation. The analysis of these graphs assures that the best response can be reached by using a low level of olefin, combined with a low level of water, a high level of polymer, and a medium level of stirring time. One can realize that these results lead to the same conclusions reached by the graph of main factors analyzed previously.

From these analyses can be defined that, to reach the high mean yield stress, a low level of O, a low level of W, and a high level of P combined with the medium level of T should be used.
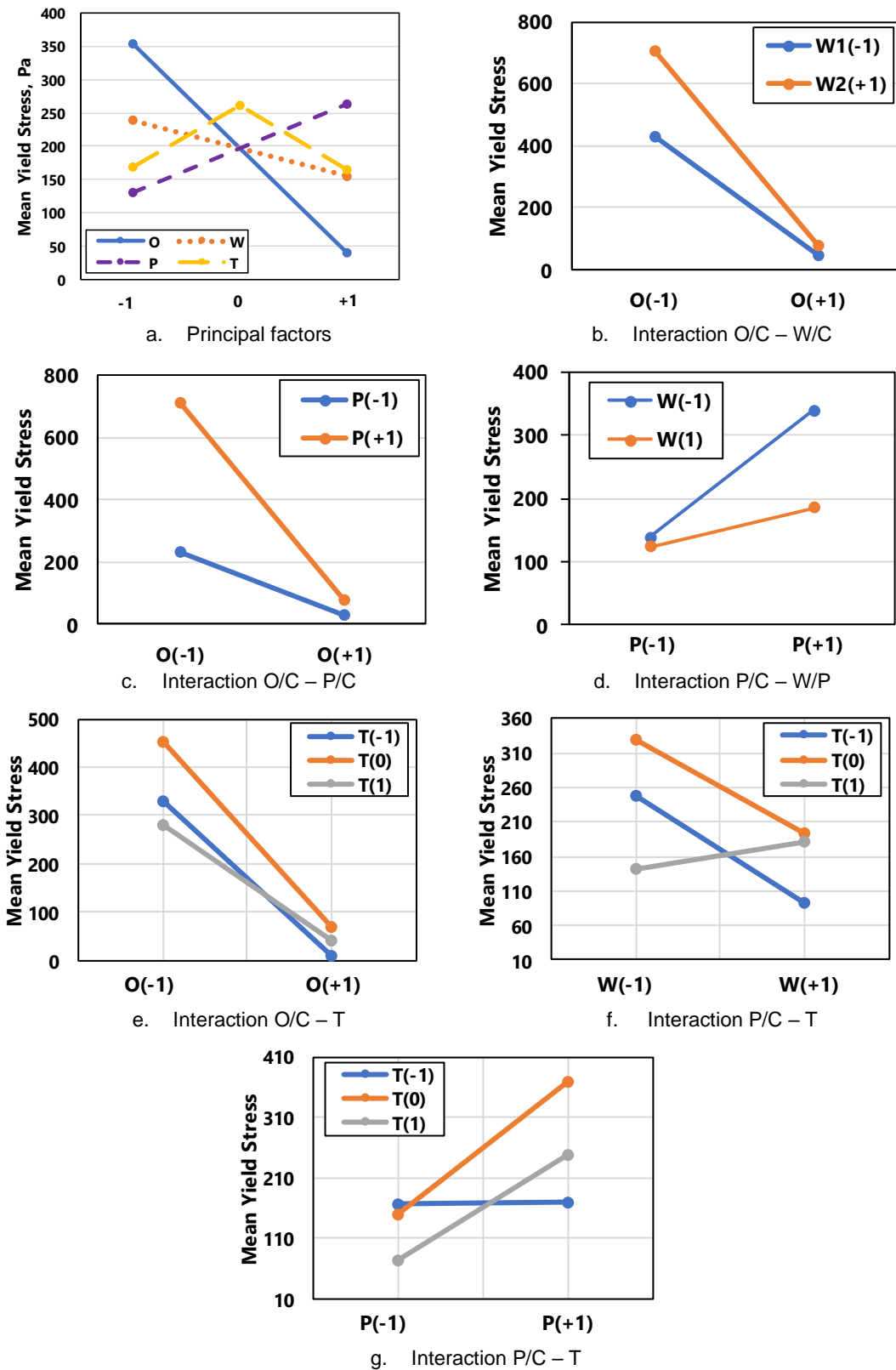
a. Principal factors

b. Interaction O/C – W/C

c. Interaction O/C – P/C

d. Interaction P/C – W/P

e. Interaction O/C – T

f. Interaction P/C – T

g. Interaction P/C – T

Figure 4.8 Graphics of principal effects and interactions

5 CONCLUSIONS AND RECOMMENDATIONS

The present work was carried out to study a shear-sensitive fluid to cure circulation loss in non-productive and highly fractured zones while drilling with synthetic fluids. Pumpability, availability of the treatment components in the platform, easy placement of material in the thief zone, and quick time to become like a paste were the motivation to develop the study this fluid. The work was divided into the design of the experiment, rheological studies, statistical analyses, and optimization of the formulation. This chapter presents the conclusions of the work developed during the present investigation and the suggestions for future studies related to the topic.

5.1 Conclusions

The conclusions of this work are divided into the sections Background and Literature Review, and Results.

5.1.1 From Background and Literature Review

The literature review showed that the treatments for lost circulation without the use of granular, foliated, or fibrous materials had been studied for several decades, and successful field tests have also been carried out where total losses have been controlled, and normal circulation of drilling fluid have been restored. The treatments used are related to crosslinked systems, gunk plugs, and shear sensitive fluids, where the latter showed less time required to control losses.

5.1.2 From Results

- The studied formulations present a solid-like behavior characterized by the oscillatory shear tests, where the G' overcame the G'' from 4 to 11 times before achieving the highest yield stress.
- The methodology used for the experimental design was adequate since the statistical analyses showed that the results did not present normality problems, and it was possible to determine a model that predicts the final response (yield stress) with a Pred R^2 of 43% of confidence.

- It was possible to identify that the olefin and the polymer (HPAM) had the most significant influence on the final yield stress within the studied levels for each factor, showing that the lower quantity of olefin leads to higher yield stress. In the same way, a higher quantity of polymer favors the higher yield stress. It was also observed that although the stirring time had no significant effect on the response, it was possible to determine that the optimum time was 90 seconds, for which the mixture resulted in higher yield stress values.

- The optimum values of variables to maximize the yield stress were determined. The best composition corresponds to the low level of O/C, low level of W/C, a high level of P/C, and an average level of stirring time.

5.2 Recommendations for future works

Among the recommendations, the following ones can be highlighted:

- Develop filtration tests to evaluate de sealing properties of the material.
- Develop and evaluate new formulations with a medium level for the factor O/C, W/C, P/C and evaluate the effect of the surfactant using at least three levels.
- Develop the rheological studies at a temperature higher than 60 °C to simulate field conditions.
- Develop studies with salt content in the formulation to evaluate its effect on Yield stress.

6 REFERENCES

AHMED, Abdelazim Abbas et al. Experimental Investigation on Co-Polymer Grafted Bentonite for Controlling Reservoir Conformance. In: 2018, SPE Kingdom of Saudi Arabia Annual Technical Symposium and Exhibition. : Society of Petroleum Engineers, 2018. Available at: https://doi.org/10.2118/192384-MS

AL-HAMEEDI, Abo Taleb T. et al. Real-time lost circulation estimation and mitigation. Egyptian Journal of Petroleum, [S. l.], v. 27, n. 4, p. 1227–1234, 2018. Available at: https://doi.org/10.1016/j.ejpe.2018.05.006

ALKINANI, Husam H. et al. Using data mining to stop or mitigate lost circulation. Journal of Petroleum Science and Engineering, [S. l.], v. 173, n. May 2018, p. 1097–1108, 2019. Available at: https://doi.org/10.1016/j.petrol.2018.10.078

ALKINANI, Husam H. et al. State-of-the-Art Review of Lost Circulation Materials and Treatments - Part II: Probability and Cost Analyses. In: 2020, International Petroleum Technology Conference. : International Petroleum Technology Conference, 2020. Available at: https://doi.org/10.2523/IPTC-19877-MS

AMOCO PRODUCTION COMPANY. Drilling Fluids Manual. Amoco Company, 1994. E-book.

AMORIM, Luciana V. Influência da Composição de Fluidos de Perfuração Sintéticos Formulados com Emulsificante Natural. In: 2017, Campina Grande. Anais [...]. Universidade Campina Grande: Campina Grande, 2017.

APALEKE, Adeleye Sami; AL-MAJED, Abdulaziz A.; HOSSAIN, Mohammed Enamul. Drilling Fluid: State of The Art and Future Trend. In: 2012, North Africa Technical Conference and Exhibition. : Society of Petroleum Engineers, 2012. p. 20–22. Available at: https://doi.org/10.2118/149555-MS

API RP 13I. Recommended Practice Standard Procedure for Laboratory Testing Drilling Fluids Recommended Practice Standard Procedure for Laboratory Testing Drilling Fluids. American Petroleum Institute, [S. l.], n. May, 2000.

ASHTER, Syed Ali. Mechanics of Materials. In: Thermoforming of Single and Multilayer Laminates. Oxford: Elsevier, 2014. p. 123–145. E-book. Available at: https://doi.org/10.1016/B978-1-4557-3172-5.00006-2

ASTON, M. S. et al. Drilling Fluids for Wellbore Strengthening. In: 2004, IADC/SPE Drilling Conference. : Society of Petroleum Engineers, 2004. p. 59–60. Available at: https://doi.org/10.2118/87130-MS

AZAR, Jamal J.; SAMUEL, Robello. Drilling engineering. Ilustrada ed. Houston: PennWell Corp, 2007. E-book.

BASSANTE, Gabriel. Análisis de las propiedades mecánicas de los elastómeros de los motores de fondo durante las operaciones de perforación en la sección 12 ¼" y en los períodos de almacenamiento. 2012. - Universidad Central de Ecuador, [s. l.], 2012.

BUSCALL, Richard; MCGOWAN, J. Ian; MORTON-JONES, Anthony J. The rheology of concentrated dispersions of weakly attracting colloidal particles with and without wall slip. Journal of Rheology, [S. l.], v. 37, n. 4, p. 621–641, 1993. Available at: https://doi.org/10.1122/1.550387

CAENN, Ryen; DARLEY, H. C. H.; GRAY, George R. Composition and Properties of Drilling and Completion Fluids. Cambridge: Elsevier, 2017. E-book. Available at: https://doi.org/10.1016/C2015-0-04159-4

CHILINGAR, George V.; VORABUTR, P. Drilling And Drilling Fluids. Canada: Elsevier, 1983. v. 11E-book.

CLINCKSPOOR, Karl Jan. Estudo estrutural, termodinâmico e cinético sobre a formação e interações de micelas gigantes em sistemas aquosos binários. 2019. - University of Campinas, Campinas, 2019.

COLLYER, A. A.; CLEGG, D. W. Rheological Measurement. Oxford: Springer Science+Business Media Dordrecht, 1988. E-book. Available at: https://doi.org/10.10071978-94-017-2898-0

DATWANI, Ali. Review of Lost Circulation Mechanisms With the Focus on Loss To Natural and Drilling Induced Fractures. 2012. - Dalhousie University. pp. 1-37, [s. l.], 2012. Available at: https://www.semanticscholar.org/paper/REVIEW-OF-LOST-CIRCULATION-MECHANISMS-WITH-THE-ON-Datwani/7149e839f93504f3ba8252f7b9944d2e1f581a2b

DEUTSCHES INSTITUT FUR NORMUNG E.V. Testing of lubricants - Testing rheological properties of lubricating greases - Part 2: Determination of flow point using an oscillatory rheometer with a parallel-plate measuring system. Liberty, MO. 2011.

DRAKE, Evelyn; CALCAVECCHIO, Peter. Shear thickening composition with polycarboxylic acid. US4663366. Concessão: 1987.

ELKATATNY, Salaheldin et al. Deep Illustration for Loss of Circulation While Drilling. Arabian Journal for Science and Engineering, [S. l.], v. 45, n. 2, p. 483–499, 2020. Available at: https://doi.org/10.1007/s13369-019-04315-6

ENERGY API. Manual de fluidos de perforación. Texas: API, 2001. E-book.

EPAARACHCHI, J. A. The effect of viscoelasticity on fatigue behaviour of polymer matrix composites. In: WOODHEAD (ed.). Creep and Fatigue in Polymer Matrix Composites. Southern Queensland, Australia Abstract: Elsevier, 2011. p. 492–513. E-book. Available at: https://doi.org/10.1533/9780857090430.3.492

EVANS, Fennell; WENNERSTROM, Hakan. The Colloidal Domain. Second ed. Minneapolis, USA: Wiley-VCH, 1999. E-book.

FERNANDES, Rubens Rosario. Relação entre o Limite de Viscoelasticidade Linear e o Limite de Escoamento de um Material Elastoviscoplástico. 2016. - Universidade Tecnológica Federal do Paraná, Paraná, 2016.

GE, Jianhao et al. The rheological properties of shear thickening fluid reinforced with SiC nanowires. Results in Physics, [S. l.], n. August, 2017. Available at: https://doi.org/10.1016/j.rinp.2017.08.065

HAMBURGER, Charles L. et al. A Shear-Thickening Fluid for Stopping Unwanted Flows While Drilling. Journal of Petroleum Technology, [S. l.], v. 37, n. 03, p. 499–504, 1985. Available at: https://doi.org/10.2118/12122-PA

HASHMAT, M. D. et al. Crosslinked Polymeric Gels as Loss Circulation Materials: An Experimental Study. In: 2016, SPE Kingdom of Saudi Arabia Annual Technical Symposium and Exhibition. : Society of Petroleum Engineers, 2016. Available at: https://doi.org/10.2118/182740-MS

HENSELER, Jörg; RINGLE, Christian M.; SINKOVICS, Rudolf R. The use of partial least squares path modeling in international marketing. In: EMERALD GROUP PUBLISHING LIMITED (ed.). Advances in International Marketing. Manchester: [s. n.], 2009. v. 20p. 277–319. E-book. Available at: https://doi.org/10.1108/S1474-7979(2009)0000020014

HOSSAIN, M. E.; ISLAM, M. R. Drilling Engineering Problems and Solutions. First ed. Hoboken, NJ, USA: John Wiley & Sons, Inc., 2018. E-book. Available at: https://doi.org/10.1002/9781118998632

HOSSAIN, M. Enamul. Fundamentals of Drilling Engineering. First ed. Hoboken, NJ, USA: John Wiley & Sons, Inc., 2016. E-book. Available at: https://doi.org/10.1002/9781119083931

HUNTER, Robert J. Foundations of Colloid Science. Second ed. Oxford: Oxford University Press, 2001. E-book.

HYUN, Kyu et al. Large amplitude oscillatory shear as a way to classify the complex fluids. Journal of Non-Newtonian Fluid Mechanics, [S. l.], v. 107, n. 1–3, p. 51–65, 2002. Available at: https://doi.org/10.1016/S0377-0257(02)00141-6

IRGENS, Fridtjov. Rheology and Non-Newtonian Fluids. Trondheim: Springer International Publishing Switzerland, 2014. E-book. Available at: https://doi.org/10.1007/978-3-319-01053-3

JIANG, Guancheng et al. Cross-linked polyacrylamide gel as loss circulation materials for combating lost circulation in high temperature well drilling operation. Journal of Petroleum Science and Engineering, [S. l.], v. 181, n. January, 2019. Available at: https://doi.org/10.1016/j.petrol.2019.106250

KRISTENSEN, Aleksander. Flow properties of water-based drilling fluids. Norway: Norwegian University of Science and Technology, 2013. E-book. Available at: http://hdl.handle.net/11250/240208

KRONBERG, Bengt; HOLMBERG, Krister; LINDMAN, Björn. Surface Chemistry of Surfactants and Polymers. Pondincherry, India: John Wiley & Sons, Ltd., 2014. v. 9781119961E-book. Available at: https://doi.org/10.1002/9781118695968

LAGALY, G.; ZIESMER, S. Colloid chemistry of clay minerals: the coagulation of montmorillonite dispersions. Advances in Colloid and Interface Science, [S. l.], v. 100–102, p. 105–128, 2003. Available at: https://doi.org/10.1016/S0001-8686(02)00064-7

LARSON, Ronald G. The structure and rheology of complex fluids. New York: Oxford University Press, 1999. E-book.

LAVROV, Alexandre. Lost circulation: Mechanisms and Solutions. Oxford: Elsevier Inc., 2016. E-book.

LENTH, Russell V. Quick and Easy Analysis of Unreplicated Factorials. Technometrics, [S. l.], v. 31, n. 4, p. 469–473, 1989. Available at: https://doi.org/10.2307/1269997

LOMBA, R. F. T. et al. Lessons learned in drilling pre-salt wells with water based muds. Proceedings of the Annual Offshore Technology Conference, [S. l.], v. 2, p. 726–736, 2013.

MABERRY, Jack; GARRISON, Greg; GARNIER, Andre. Shear-sensitive plugging fluid for plugging and a method for plugging a subterranean formation zone. US 6818598 B2. Concessão: 2004.

MARQUES, D. C. et al. Thermodynamic Behavior of Olefin and Methane Mixtures Applied to Synthetic Drilling Fluids Well Control. SPE Drilling & Completion 33, v. 3, p. 230–240, 2017. Available at: https://doi.org/10.2118/185470-PA

MEZGER, Thomas G. The rheology handbook. 4. ed. Germany: Vincentz Network GmbH & Co. KG, 2014. E-book.

MINTZ, Donald; IRANI, Cyrus. Shear thickening well control fluid. US4391925A. Concessão: 1983.

MIRANDA, C. R. et al. Materials for Controlling Severe Lost Circulation - Laboratory Evaluation. SPE Latin America and Caribbean Petroleum Engineering Conference, [S. l.], p. 1–13, 2017. Available at: https://doi.org/10.2118/185582-MS

MITCHELL, Robert F.; MISKA, Stefan Z. **Fundamentals of Drilling Engineering**. Beverly:

Scrivener Publishing LLC, 2011. v. 12*E-book*.

MONTGOMERY, Douglas C. Introduccion a los diseños factoriales. In: NORIEGA, Grupo (ed.). Diseño y análisis de experimentos. Segunda ed ed. Mexico: Limusa, 2004. p. 170–422. E-book.

NEFF, J. M.; MCKELVIE, S.; AYERS, R. C. Environmental Impacts of Synthetic Based Drilling Fluids. Houston: [s. n.], 2000.

NETO, Benicio de Barros; SCARMINIO, Ieda Spacino; BRUNS, Roy Edward. Como fazer experimentos. Editora da ed. Campinas: Campinas, 2001. E-book.

PINHEIRO, R. S. et al. Well Construction Challenges in the Pre-Salt Development Projects. [S. l.], n. May, p. 4–7, 2015.

PULIDO, Humerto Gutierrés; SALAZAR, Román de la Vara. Análisis y diseño de experimentos. Tercera ed ed. Mc Graw Hill, 2012. E-book.

RAHMAN, Mehreen. Study of pre-shearing protocol and rheological parameters of shear thickening fluids containing nano particles. 2000. - Thapar University. pp. 1-22, [s. l.], 2000. Available at: https://doi.org/10.1201/9781420039283.fmatt

RIBEIRO, Priscilla. Posicionamento de tampões em poços de petróleo: uma investigação de escoamentos de inversão por gravidade. [S. l.], p. 208, 2017.

ROMERO-ZERON, Laura; MANALO, F.; KANTZAS, A. Characterization of Crosslinked Gel Kinetics and Gel Strength Using NMR. In: 2004, SPE International Symposium and Exhibition on Formation Damage Control. : Society of Petroleum Engineers, 2004. Available at: https://doi.org/10.2118/86548-MS

ROY, Debjani; AUDUS, Debra J.; MIGLER, Kalman B. Rheology of crystallizing polymers : The role of spherulitic superstructures , gap height , and nucleation densities. Journal of Rheology, [S. l.], v. 63, n. 851, p. 862, 2019. Available at: https://doi.org/10.1122/1.5109893

SHAARPOUR, Mano. Lost circulation material blend offering high fluid loss with minimum solids. US 2004 / 0244978A1. Concessão: 2004.

SHAHBAZI, Khalil; NAZEMI, Rasoul. A comprehensive review on selection of lost circulation materials for fractured oil reservoirs. ISERD International Conference, Istanbul, Turkey, [S. l.], p. 19–25, 2018.

SONG, Ranran; JIANG, Guancheng; WANG, Kai. Gelation mechanism and rheological properties of polyacrylamide crosslinking with polyethyleneimine and its plugging performance in air-foam displacement. [S. l.], v. 45778, p. 1–11, 2018. Available at: https://doi.org/10.1002/app.45778

SUNDE, Egil; KONRAD, Hans. Plugging liquid for plugging a subterranean formation zone. US5919739. Concessão: 1986.

TEIXEIRA, G. T. et al. New material for wellbore strengthening and fluid losses mitigation in deepwater drilling scenario. Society of Petroleum Engineers - SPE Deepwater Drilling and Completions Conference 2014, [S. l.], p. 128–139, 2014. Available at: https://doi.org/10.2118/170266-ms

UETANI, Takaaki et al. Experimental Investigation of Crude-Oil Emulsion Stability: Effect of Oil and Brine Compositions, Asphaltene, Wax, Toluene Insolubles, Temperature, Shear Stress, and Water Cut. SPE Production & Operations, [S. l.], v. 35, n. 02, p. 320–334, 2020. Available at: https://doi.org/10.2118/192064-PA

VERRET, Robin. Method for decreasing lost circulation during well operation. US6976537B1. Concessão: 2005.

WALLS, H. J. et al. Yield stress and wall slip phenomena in colloidal silica gels Published by

the The Society of Rheology. [S. l.], v. 847, 2003. Available at: https://doi.org/10.1122/1.1574023

XIE, Mingliang et al. A New Mechanistic Approach to Simulating Swelling Processes in Bentonite Materials. In: Elsevier Geo-Engineering Book Series. Elsevier, 2004. v. 2p. 323–328. E-book. Available at: https://doi.org/10.1016/S1571-9960(04)80061-2

APPENDIX A   SOME PROPERTIES OF SURFACTANTS, BENTONITE AND POLYMERS

A.1. Emulsions

Emulsions can be formed by condensation or dispersion methods (Ultrasonication, high-speed stirring, shaking of the two-phase liquid mixture) as solids in liquids or liquid in liquid dispersions (Fig. A-1). High energy is required to form a stable emulsion, while spontaneous emulsification can undergo if a two-phase system is provided by a third component (surface active agent), which lowers the interfacial tension close to zero. The result is a more or less spherical vesicle when the bilayer array encloses an aqueous region (Fig. A-1 a), where the wall thickness is about twice the chain length, and there is water on both sides of the surfactant. A separate pure oil region in the interior of a continuous water phase (Fig. A-1 b) is usually generated using two surfactants, one ionic and one neutral dipolar compound of similar chain length (HUNTER, 2001).
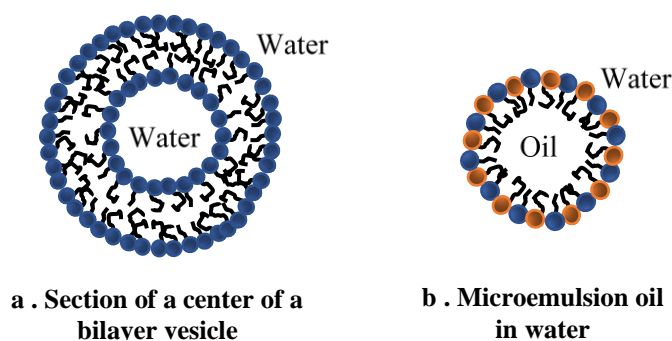

a . Section of a center of a bilaver vesicle   **b . Microemulsion oil in water**

Fig. A-1. Liquid in liquid emulsions. Adapted from: Hunter, 2001

Emulsions are less stable at a higher temperature because the heat increases the movement of water droplets and promotes coalescence, besides reducing the oil viscosity and thus allowing the particles to move more quickly. (UETANI *et al.*, 2020).

A.2. Surfactants

A general class of substances called amphiphiles consist in two well-defined regions (Fig. A-2 a), one of that is lipophilic (head) that is non-polar and usually consist of aliphatic or aromatic hydrocarbons and hydrophilic one (tail) that consist of polar groups which can interact actively with water (HUNTER, 2001).
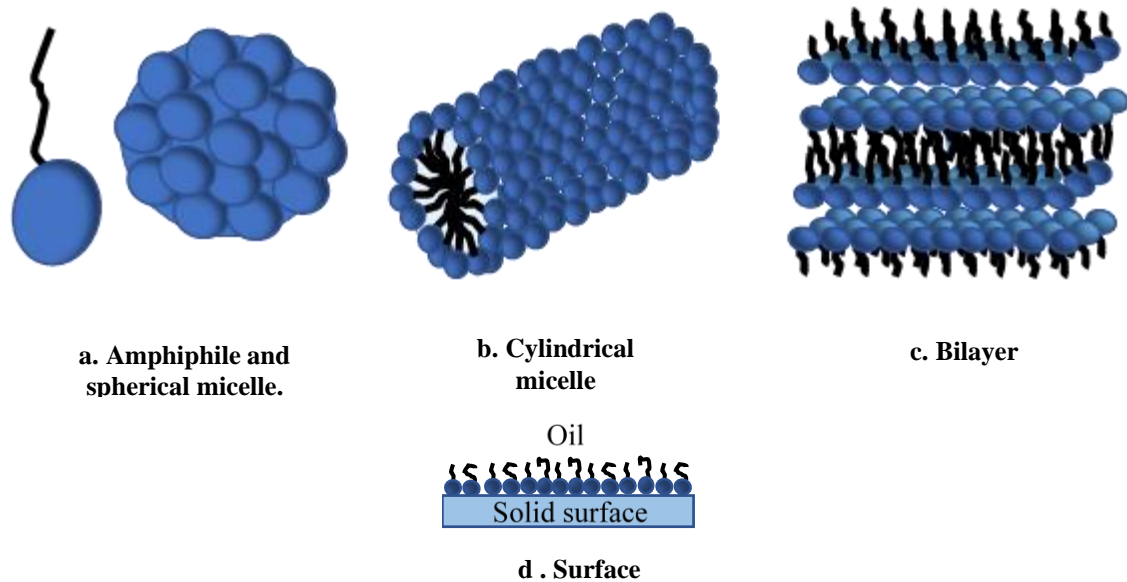
a. Amphiphile and spherical micelle.   **b. Cylindrical micelle**   **c. Bilayer**

Oil

Solid surface

d . Surface

Fig. A-2. Conventional representations for micelles and surface modification. Adapted from: Hunter, 2001

Commercial surface-active agents (surfactants) are used for various purposes, like detergent, colloidal stabilizer, and wetting agent (HUNTER, 2001).

As the concentration of the surfactant increases, the molecules packed close together, and the interactions between hydrophobic chains tend to stick, forming micelles; the concentration at which micelles first form in the solution is called critical micelle concentration (CMC). These structures form regions from which the solvent is excluded. Usually, the first well-defined structure of micelles is spherical (Fig. A-2 a). However, as the surfactant concentration increases, the shape of the spherical micelles become distorted and forms cylindrical rods (Fig. A-2b) or disks. Under special conditions, two aqueous bilayers separated regions can be formed, similar to a biological membrane (Fig. A-2 c) (HUNTER, 2001).

For solid in liquid emulsions, the modification of solid surface can be achieved by an adsorbed layer of reactive surfactant on the surface, where surfactants molecules are attached as a thin film (Fig. A-2 d). This way, hydrophilic surfaces can be made hydrophobic, or a specific functionality can be introduced (KRONBERG; HOLMBERG; LINDMAN, 2014).

A.3. Bentonite Clay Minerals

Clay particles are used in drilling fluids to increase the gel strength or the fluid weight to control hydrostatic pressure and filtration problems in the drilled zone.

Solute and solvent molecules are of comparable size in standard solutions, and typically, solute molecules are assumed to be dispersed uniformly throughout the solvent. There is an important class of materials in which the units dispersed through the solvent are much larger than the solvent molecules. These systems are called colloidal dispersions, and they may arise in a variety of ways, in which one or more of the components has at least one dimension between 1 nm and 1000 nm (HUNTER, 2001).
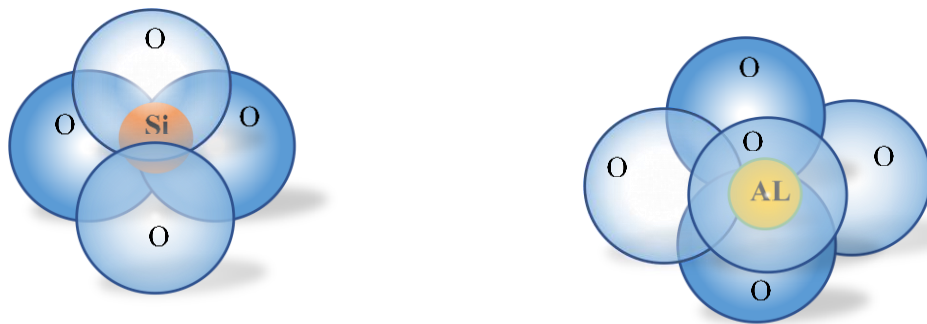
a . Arrangement of silica tetrahedron   **b . Arrangement of Aluminum octahedron**

Fig. A-3. Basics arrangement for silica and aluminum

Montmorillonite (the principal bentonite component) is the most abundant minerals within the smectite group of 2:1 clay minerals (one octahedral sheet sandwich between two tetrahedral sheets) (Fig. A-3). Montmorillonite particles may be as small as 0,1 μm in diameter and irregular shape; they are foliated and compact; the particles are like assemblages of silicate layers, where the charges of the layers result from isomorphous substitution. The edges of the layers show silanol and aluminum groups. These groups are positively charged at low pH, negatively charged at high pH, accepted as having zero charge at the pH near 5, according to several colloid chemical arguments (LAGALY; ZIESMER, 2003).
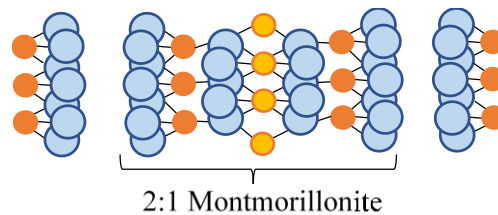

2:1 Montmorillonite

Fig. A-4. Bentonite triple sheet

The swelling mechanism of bentonites results from the new embedding of water molecules into the triple sheet molecule of montmorillonite(Fig. A-4). This mechanism is helped by the interlayer cations dissociation (Na^+, K^+, Ca^{2+}), where the water fills this space.

When the water content increases, the thickness interlayers increase, and if the water contains ions, the swelling decreases due to the cation exchange process (Fig. A-5). That occurs between the ions in the solution and the ions in the interlayer region (HUNTER, 2001; XIE *et al.*, 2004).
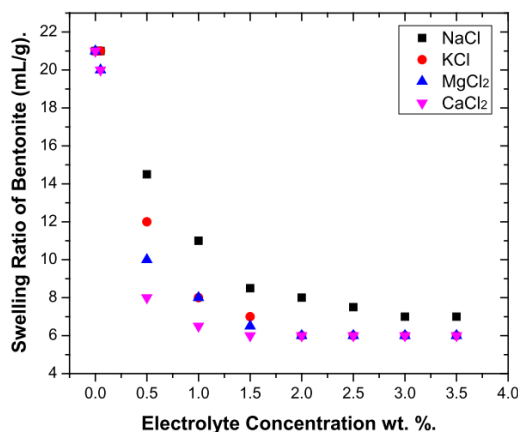

Fig. A-5. Effect of salts in swelling ratio of bentonite. Source: (AHMED *et al.*, 2018)

A.4. Polymers

One of the uses of polymers is to control the rheological properties of a colloidal dispersion. Generally, the rheology is related to how the system responds to a mechanical perturbation in terms of the viscous flow (associated with liquids) and the elastic deformation (associated with solids), and how both related to each other at different scales. Colloid systems typically show a behavior between solid and liquid and present both elastic and viscous behavior, where the non-Newtonian regimen is characteristic (EVANS; WENNERSTROM, 1999).

In colloidal systems, the polymer will adsorb to a surface (Fig. A-6) and make many contacts with it, resulting in high adsorption energy. A loss of configurational entropy compensates that, but if the monomers have some affinity to the surface, the polymer will adsorb strongly and irreversibly. A block copolymer under bad solvent conditions strongly tends for adsorption, and a polyelectrolyte adsorbs strongly on an oppositely charged surface caused by electrostatic forces. Finally, the polymer chain can adsorb to the surface by a covalent bond (EVANS; WENNERSTROM, 1999).
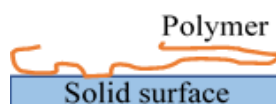

Fig. A-6. Polymer Adsorption

APPENDIX B   SELECTION OF THE GAP BETWEEN THE PLATES OF THE RHEOMETER

The procedure for the formulation was defined to select the optimum gap from 0.5 mm, 0.8 mm, and 1.0 mm plate separation. Fig. B-1 a, shows the measurement observed from stress between the three studied height. With a visual analysis, it shows that for 0.8 mm, the curve has higher results than the others; this is verified with the calculation of yield point. For Fig. B-1 b, a visual analysis indicates that the 0.5 mm and 0.8 mm curves are close, but for the yield point the results are different.
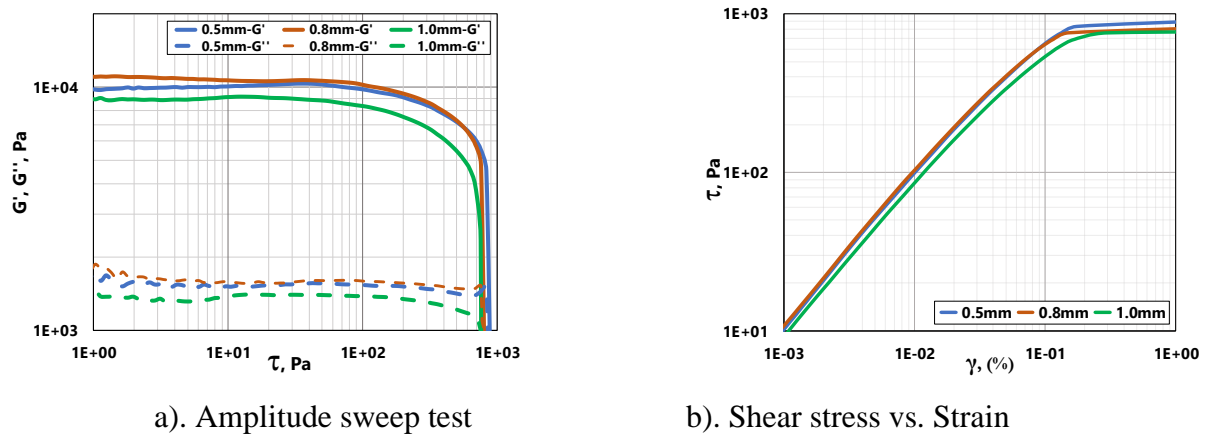

a). Amplitude sweep test   b). Shear stress vs. Strain

Fig. B-1. Tests to gap selection for bentonite

The mean yield point calculated is shown in Tab B-1, to define which could be the most appropriate gap for the studies. For the bentonite formulation, visually, no suitable clearance can be chosen for the three curves, so the analysis was complemented by comparing the yield stress for the three gaps, the closest values corresponds to 0.8 mm and 1.0 mm, then for this formulation is confirm that a gap of 0.8 mm should be used confidently, and for the next analyses this gap is used.

Tab B-1 Yield point for the different gap between plates

GAP	τ. Pa
0.5	220.28
0.8	163.17
1.0	140.70

APPENDIX C   IDEAL MODELS FOR VISCOELASTIC MATERIALS

The stress applied to viscoelastic materials undergoes microscopic and macroscopic deformations. It presents an instantaneous deformation that could be either elastic or elastic and plastic. When stress is removed, the elastic deformation disappears, while the plastic deformation remains. There are some ideal mathematical models that explain the behavior of viscoelastic materials under the linear viscoelastic region (LVR). Among them, the Maxwell model and the Kelvin-Voigt model are the simplest and uses a spring to represent the elastic behavior and a dashpot to represent the viscous behavior (FERNANDES, 2016).
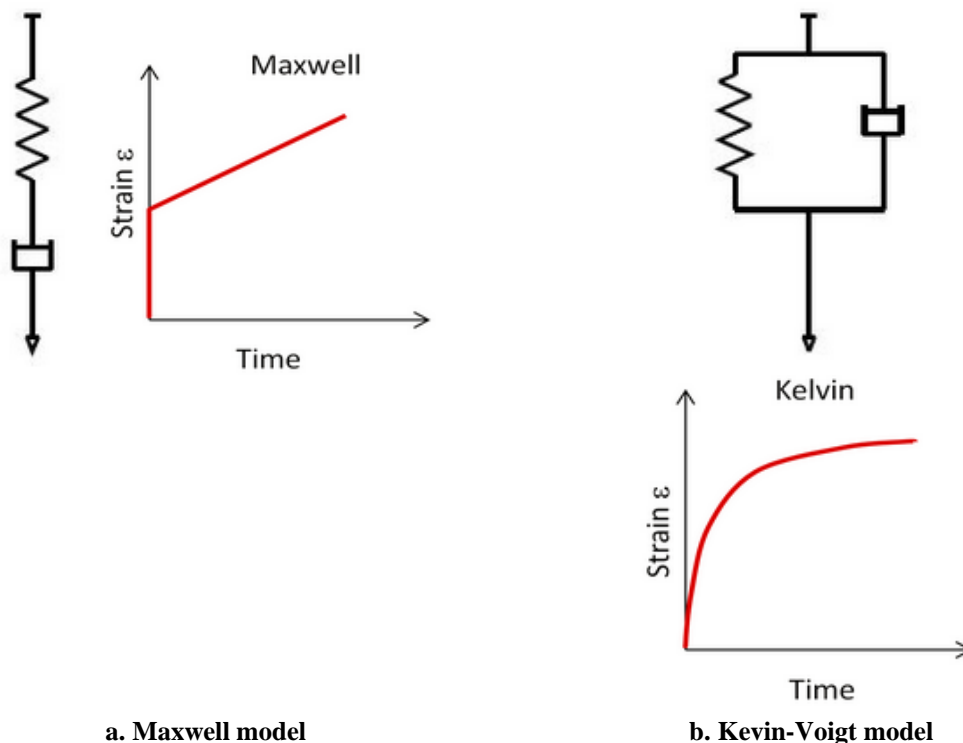

a. Maxwell model   **b. Kevin-Voigt model**
Fig. C-1 Representation of ideal models for viscoelastic behavior. Source: Adapted from (ASHTER, 2014; EPAARACHCHI, 2011)

Fig. C-1 shows the response of an experiment where stress is applied over the time it represents the viscoelastic response of the two ideal models (Maxwell and Kelvin-Voigt).

Fig. C-1a represents the Maxwell model where the component is in series, and can be described with the Eq. C-1 (creep response), and Eq. C-2 (relaxation response), where ε is the normal strain, σ is the shear stress, E is the modulus of the spring , η is the apparent viscosity, t is the time, and λ is the relaxation time. This model present some disadvantages,

under constant stress, the deformation increase unlimited as time increases, and the applied stress decay to zero at infinite time, which for viscoelastic materials is not true (ASHTER, 2014; EPAARACHCHI, 2011).

$$\varepsilon(t) = \frac{\sigma_0}{E}\left(1 + \frac{t}{\lambda}\right), where\ \lambda = \frac{\eta}{E}$$
$$\textbf{Eq. C-1}$$

$$\sigma(t) = \sigma_0 \exp(-t/\lambda)$$
$$\textbf{Eq. C-2}$$

Fig. C-1b represents the Kelvin-Voigt model that comprises a parallel arrangement, where the model exhibits the primary creep phenomenon but can not demonstrate a steady-state stress relaxation, described by Eq. C-3 and Eq. C-4 (ASHTER, 2014; EPAARACHCHI, 2011).

$$\varepsilon(t) = \frac{\sigma_0}{E}[(1 - \exp(-t/\lambda))]$$
$$\textbf{Eq. C-3}$$

$$\sigma(t) = No\ relaxation\ occurs$$
$$\textbf{Eq. C-4}$$

APPENDIX D MATLAB CODE FOR STATISTICAL ANALYSES

The next code serves to solve the design of experiments for n number of factors and maximum of three levels for each factor.

```
clear all
clc
% Indicate the address of the file, the sheet and the range
A = xlsread('DOE George', 'Elastic','A2:E25');
% Define the confidence level alpha normally 95%
alpha = 0.05;
%% To Codify the matrix for develop the model: Checks if there are two unique
% values (levels). If so, attributes -1 to the lowest and +1 to the highest
% If there are 3 levels, -1, 0, +1 respectively. If your factors are
% codified this step may be ignored.
for j=1:size(A,2)-1
div=(max(A(:,j))-min(A(:,j)))/2;
prom=mean(A(:,j));
   for i=1:size(A,1)
      A(i,j)=((A(i,j))-prom)/div;
   end
end
%% To define a new matrix X that contains only the codified levels
% Get elements except last column
X = [A(:,(1:size(A,2)-1))];
% To define ALL possible combinations of the factors
% Interaction of col 1 and 2 is element-wise multiplication of col 1 and
% col 2, and so on.
% Will contain the new interactions and old factors
Tab = X;
% Number of factors
nFac = size(A,2)-1;
% Vector to iterate through factors
vecFact = 1:nFac;
% Table for principal factors, each row represent a column of the
% interaction in X
Tabcomb = zeros(nFac,nFac);
% Possible combinations between factors
Combin = nchoosek(vecFact,1);
% Table for define the number of possible combination of factors
for i = 1:size(Combin,1)
   for j = 1:size(Combin,2)
        Tabcomb(i,j) = [Combin(i,j)];
```

```
        end
      end
% Number of the last row to create the interaction between factors
tc = size(Tabcomb,1);
% Get the k-th order of combinations (k=2 is second order, etc.)
for k = 2:size(A,2)-1;
    % Used as accountant
    n = 1;
    % Possible combinations
    Combin = nchoosek(vecFact,k);
    for i = 1:size(Combin,1)
        for j = 1:size(Combin,2);
            % To place and indicate the interactions
            Tabcomb(tc+1,j) = [Combin(i,j)];
        end
        tc = tc+1;
    end
    % To create the matrix of interactions
    % For Colums
    for Cols = 1:size(Combin,1)
        % For files
        for row = 1:size(X,1);
            Prod1 = X(row,Combin(Cols,1));
            if size(Combin,2)>1
                Prod2 = X(row,Combin(Cols,2))*Prod1;
                % For products from 3th column of Combin
                for m = 3:size(Combin,2)
                        Prod3 = X(row,Combin(Cols,m))*Prod2;
                        Prod2 = Prod3 ;
                end
            else
                Prod2 = 1;
                Prod3 = X(row,Combin(Cols,1));
                Prod2 = Prod3 ;
            end
            %Matrix with interactions
            X(row,size(Tab,2)+n) = Prod2;
        end
        n = n+1;
    end
    Tab = X;
end;
% To define exactly the interactions of factors, each row corresponds to a
% colum of interaction in X
Tabcomb(1:size(Tabcomb,1),size(Tabcomb,2)+1) = [1:size(Tabcomb,1)];
%% TO DELETE ROWS/COLUMNS FROM THE FINAL MATRIX OF
INTERACTIONS
% Used to remove outliers or factors/combinations of factors from the final
% calculation
%  Remove the '%' and write the number of the column/row to delete
```

```
%
% To delete columns, ex. [a b c]
%
% dc = [4 5 7 8 11 12 13 14 15];
% X(:,dc) = []
% Tabcomb(dc,:) = [];
%
% To delete rows, ex. [a b c]
%
% dr = [5 6]
% X(dr,:) = []
% A(dr,:) = []
%
% IMPORTANT!
% ACTIVATE Tabcomb when remove columns or rows!**
% Tabcomb(1:size(Tabcomb,1),size(Tabcomb,2)+1)=[1:size(Tabcomb,1)];

%% Matrix to find the coefficients of the model
% Typical solution to a linear system of the form y = Xb, where y are the
% measured values, X are the coefficients and interactions and b are the
% unknown coefficients
% Final matrix to calculate the model
X = [ones(size(X,1),1) X];
% To define the column of the response
y = [A(:,size(A,2))];
% To gets the coefficients of the model
b = inv(X'*X)*X'*y;

%% EFFECTS
% The intercept effect is the same as the first coefficient.
% The remaining effects are twice the coefficients.
Effect = zeros(size(b,1),1);
Effect(1,1)=b(1,1);
 for n = 2:size(b,1)
     Effect(n,1)= b(n,1)*2;
 end
%Predicted Model
 % Can be calculated by remembering the initial equation y = Xb
y_calc = X*b;
%Residuals
e = y - y_calc;

 %% ANOVA,
% It is necessary to define the columns where are the principal factor in
% the matrix A. ex. [A(:,3)]
% Requires customization for each use case.
[p,tbl,stats,terms] = anovan(A(:,size(A,2)),{[A(:,1)] [A(:,2)] [A(:,3)]...
   [A(:,4)]},'model','interaction');
% Sum of Squares of all data
SS = cell2mat(tbl([2:size(tbl)],2));
```

```matlab
% Mean square: Sum of squares divided by degree of freedom
SSM = cell2mat(tbl([2:size(tbl)],5));
% Total sum of squares
SST = cell2mat(tbl(size(tbl,1),2));
% R^2: Sum of squares, excluding error and total
SSP=sum(SS([1:size(SS,1)-2],1));
R2 = SSP/SS(size(SS,1));
% R^2(Adjusted): considers the number of degrees of freedom.
Radjus = 1- SSM(size(SSM,1))/(SS(size(SS,1))/cell2mat(tbl(size(tbl,1),3)));
% R^2(predicted)
% Calculuis of PRESS(predicted residual error sum of squares)
%Hat Matrix H, for PRESS calculus
H = X*inv(X'*X)*X';
h = diag (H);
if sum(e)== 0
   PRESS = 0;
else
   PRESS = zeros(size(H,1),1);
   for i=1:size(PRESS,1)
     if h(i,1)==1
        PRESS(i,1)= 0;
     else
        PRESS(i,1)=(e(i,1)/(1-h(i,1)))^2;
     end
   end
end
Rpred = 1-sum(sum(PRESS(:,1)))/SST;
if Rpred < 0
   Rpred = 0;
else
   Rpred = Rpred;
end
%% Predicted vs calculated plot
figure1 = figure;
   % Create axes
axes1 = axes('Parent',figure1);
hold(axes1,'on');
   % Set the remaining axes properties
set(axes1,'FontSize',12,'FontWeight','bold');

% Create plot
subplot(2,3,3),scatter(y,y_calc,'DisplayName','y_calc vs y',...
   'MarkerFaceColor',[0 0 0],...
   'MarkerEdgeColor',[0 0 0],...
   'Marker','pentagram');
% Plot a perfect correlation between y_calc and y
line([min(y) max(y)],[min(y) max(y)],'LineWidth',2,'Color',[1 0 0]);
ylabel('y_c_a_l');
xlabel('y_m_e_d');
title('y_c_a_l_c vs y_m_e_d');
```

```matlab
% Add numbers to indentify each data point.
   for i = 1:size(X, 1)
   text(y(i), y_calc(i), num2str(i));
   end
   hold off
%
%Normal distribution of effects
subplot(2,3,1),normplot(e);
xlabel('Residuals')
%
%Residual versus predicted
subplot(2,3,2)  % 2 x 2 graph, plot on the 3rd position
scatter(y_calc,e,'DisplayName','y_calc vs y_meas','MarkerFaceColor',...
   [0 0 0],'MarkerEdgeColor',[0 0 0],'Marker','pentagram')
ylabel('Residuals')
xlabel('Predicted')
line([min(y_calc)-100 max(y_calc)+100],[0 0],'LineWidth',2,'Color',[1 0 0]);
title('Residuals vs predicted');
%
% Margin error by Lenth method (1983) for Pareto plot
sE = sort(abs(Effect([2:size(Effect,1)],1)),'ascend');
So1 = 1.5*median(sE);
SO = 2.5*So1;
sE2 = zeros(size(sE,1),1);
for i = 1:size(sE,1)
   if sE(i,1)<SO
      sE2(i,1) =  sE(i,1);
   else
      sE2(i,1) = 0;
   end

end
So2 = median(sE2(sE2>0));
PSE = 1.5*So2;
Gl2 = (size(Effect,1)-1)/3;
Ts1 = tinv((1-alpha/2),Gl2);
%Margin error
ME = Ts1*PSE;
alfa2 = (1-0.95^(1/(size(Effect,1)-1)))/2;
Ts2 = tinv((1-alfa2/2),Gl2);
ME2 = Ts2*PSE;
%
%Pareto plot
subplot(2,3,4),barh(abs(Effect([2:size(Effect,1)],1)));
line([ME ME],[0 size(Effect,1)],'LineWidth',2,'Color',[1 0 0]);
   %line([ME2 ME2],[0 size(E,1)],'LineWidth',2,'Color',[1 0 0]);
title('Pareto Chart');
ylabel('Term');
xlabel('Effects');
%
```

```
% Create textbox with quality of fit parameters R^2, R^2(Adj), R^2(pred)
annotation(figure1,'textbox',...
    [0.441 0.14070351758794 0.182703703703704 0.298994974874372],...
    'String',{strcat('R2=',string(R2)),strcat('Radjus=',...
    string(Radjus)), strcat('Rpred=',string(Rpred))},...
    'FontSize',12,'FitBoxToText','off','BackgroundColor',[1 1 1]);
% Interaction factors useful to identify the interactions deleted, the last
% Shows the table of interactions to relate with the pareto plot
Tabcomb
```